Accepted Manuscript

Purple acid phosphatase inhibitors as leads for osteoporosis chemotherapeutics

Waleed M. Hussein, Daniel Feder, Gerhard Schenk, Luke W. Guddat, Ross P. McGeary

PII: S0223-5234(18)30659-7

DOI: 10.1016/j.ejmech.2018.08.004

Reference: EJMECH 10615

To appear in: *European Journal of Medicinal Chemistry*

Received Date: 23 April 2018

Revised Date: 14 June 2018

Accepted Date: 1 August 2018

Please cite this article as: W.M. Hussein, D. Feder, G. Schenk, L.W. Guddat, R.P. McGeary, Purple acid phosphatase inhibitors as leads for osteoporosis chemotherapeutics, *European Journal of Medicinal Chemistry* (2018), doi: 10.1016/j.ejmech.2018.08.004.

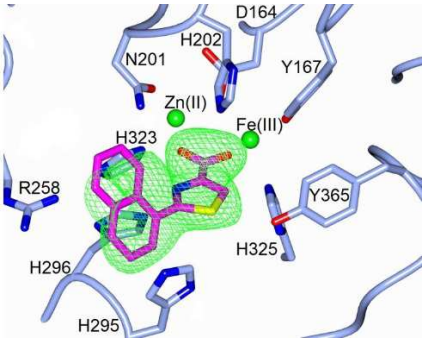

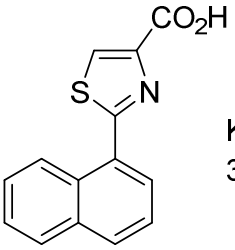

K_i (pig PAP)
33 μM

Inhibitors of
Purple Acid Phosphatase

Graphical Abstract **Revised Manuscript EJMECH-D-18-01046**

Purple acid phosphatase inhibitors as leads for osteoporosis chemotherapeutics

Waleed M. Hussein[a,b], Daniel Feder[a], Gerhard Schenk[a], Luke W. Guddat[a] and Ross P. McGeary[a,*]

[a]The University of Queensland, School of Chemistry and Molecular Biosciences, Brisbane, QLD 4072, Australia

[b]Helwan University, Pharmaceutical Organic Chemistry Department, Faculty of Pharmacy, Ein Helwan, Helwan, Egypt

*Corresponding author: E-mail address r.mcgeary@uq.edu.au

Key Words: Purple acid phosphatase, Tartrate-resistant acid phosphatase, Metallohydrolases, Chemotherapeutics, Osteoporosis.

Abstract:

Purple acid phosphatases (PAPs) are metalloenzymes that catalyse the hydrolysis of phosphate esters under acidic conditions. Their active site contains a Fe(III)Fe(II) metal centre in mammals and a Fe(III)Zn(II) or Fe(III)Mn(II) metal centre in plants. In humans, elevated PAP levels in serum strongly correlate with the progression of osteoporosis and metabolic bone malignancies, which make PAP a target suitable for the development of chemotherapeutics to combat bone ailments. Due to difficulties in obtaining the human enzyme, the corresponding enzymes from red kidney bean and pig have been used previously to develop specific PAP inhibitors. Here, existing lead compounds were further elaborated to create a series of inhibitors with K_i values as low as ~30 μM. The inhibition constants of these compounds were of comparable magnitude for pig and red kidney bean PAPs, indicating that relevant binding interactions are conserved. The crystal structure of red kidney bean PAP in complex with the most potent inhibitor in this series, compound **4f**, was solved to 2.40 Å resolution. This inhibitor coordinates directly to the binuclear metal centre in the active site as expected based on its competitive mode of inhibition. Docking simulations predict that this compound binds to human PAP in a similar mode. This study presents the first example of a PAP structure in complex with an inhibitor that is of relevance to the development of anti-osteoporotic chemotherapeutics.

1. Introduction

Purple acid phosphatases (PAPs, also referred to as tartrate-resistant acid phosphatases) are metalloenzymes found in animals, plants and fungi [1-5]. They utilise a binuclear metal centre to catalyse the hydrolysis of phosphate esters and anhydrides under acidic conditions, with an optimal pH ~5 [6-12]. The overall reaction is given in Equation 1.

$$RO\text{-}PO_3^{2-} + H_2O \longrightarrow ROH + HPO_4^{2-}$$ Equation 1

PAPs are non-specific enzymes that can dephosphorylate diverse substrates, including ATP, ADP and *para*-nitrophenyl phosphate (*p*NPP) [1-4, 13], as well as phosphoproteins such as osteopontin and bone sialoprotein [14-15]. Several roles for mammalian PAPs have been suggested. Pig PAP found in the allantoic fluid of pregnant sows is believed to transport iron from the mother to the foetus during gestation [16], and therefore the enzyme is also referred to as uteroferrin [6, 17-19]. In humans, PAP function appears to be tissue-specific; the enzyme is involved in the inflammatory response of antigen-presenting cells [20], as well as in bone resorptive processes in osteoclasts [15, 21]. The diverse roles of mammalian PAP are associated with the enzyme's bifunctional character; apart from its hydrolytic activity it can also act as a Fenton catalyst due to the presence of its redox active Fe(III)Fe(II/III) centre [22]. It has been hypothesised that the reactive oxygen species (ROS)-generating activity of PAP could play a role in collagen degradation [23]. Although the substrate(s) of PAP in bone tissue is unknown, studies with transgenic mice clearly established the enzyme's function in bone turnover. Mice overexpressing the PAP gene are found to be osteoporotic [14] and show an increase in bone turnover [24]. In contrast, mice deficient in PAP display a phenotype characteristic of osteopetrosis [24], with increased bone mineral density, abnormal ossification [14] and defects in the resorption and mineralisation of growing bone [25]. Thus, PAP has emerged as a target for inhibitors that may lead to the development of novel treatments for osteoporosis, bone malignancies and metabolic bone diseases.

In the absence of effective recombinant expression systems for human PAP the enzymes extracted from pig uterine fluid (*i.e.* uteroferrin) and red kidney bean PAP (rkbPAP) have been used as models to test the efficacy of inhibitors. Despite the modest sequence similarity between rkbPAP and mammalian PAPs [26-27] its inclusion into an inhibitor design program is warranted on the basis of similar (i) substrate specificities, (ii) interactions with known

inhibitors and (iii) mechanism [19, 28-29]. A number of thiol and phosphonate compounds with IC_{50} values 80–3000 μM have been developed [30]; similar IC_{50} values were reported for a series of phosphotyrosine-containing tripeptides [28]. Our group reported a series of α-alkoxynaphthylmethylphosphonic acids [31], acyl derivatives of α-aminonaphthylmethyl phosphonic acid [32] and acyl derivatives of 6-aminopenicillanic acid [33] as inhibitors of PAP with K_i and IC_{50} values in the low micromolar range. We also employed a fragment-based screening approach to identify three potential inhibitor leads; crystal structures provided insight about the mode of their binding in the active site of rkbPAP [27]. Here, we used these fragments as starting points for the design of a new series of inhibitors with improved binding interactions.

2. Results and Discussion

Inhibitor synthesis: In a previous study, four fragments from a Maybridge™ library were identified as promising inhibitor leads for PAPs [27]. The molecular structures of these compounds (*i.e.* **1**, **2**, **3** and **4a**) are shown in Figure 1. The crystal structures of rkbPAP in complex with compounds **2** and **4a** (competitive inhibitors with K_i values of 43 μM and 340 μM for rkbPAP and 59 μM and 42 μM pig PAP, respectively [27]) demonstrate that the active site of the enzyme offers numerous structural features to allow further elaboration of inhibitor molecules with high affinity and specificity (Figure 1).

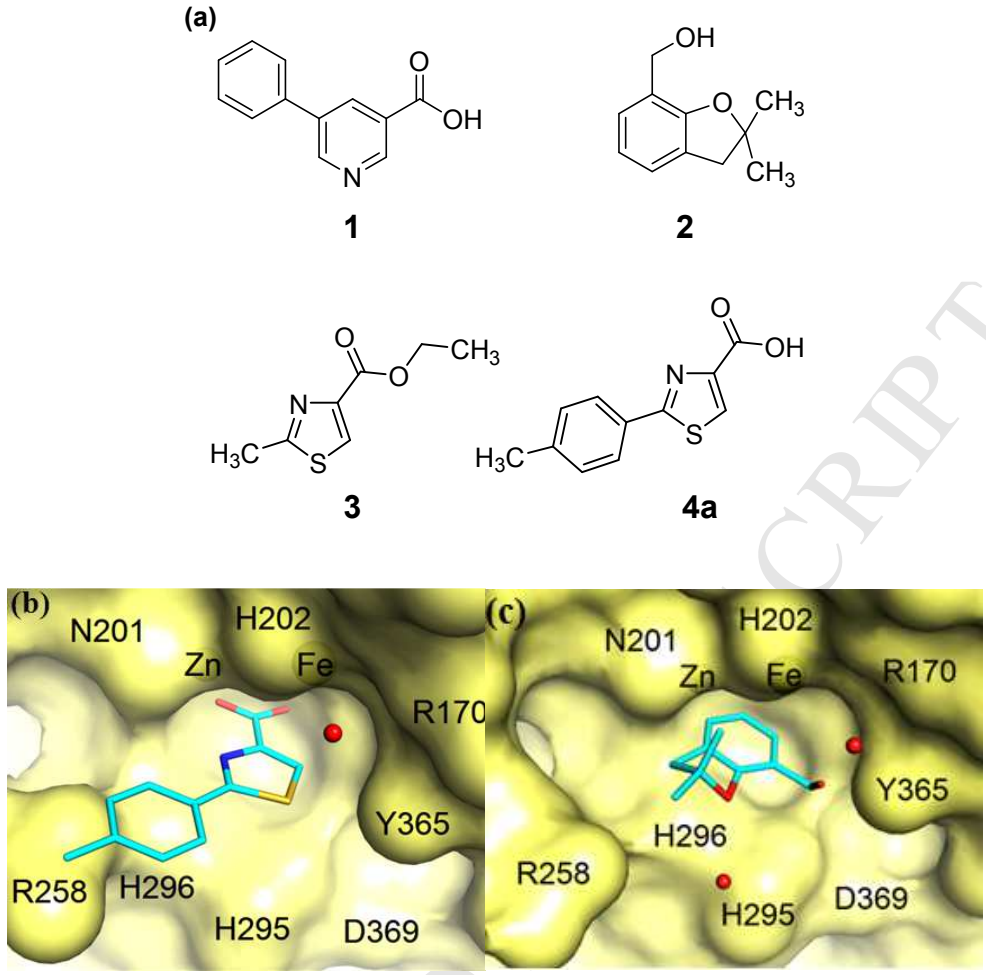

Figure 1: (a) Four fragments identified from a Maybridge™ compound library as PAP inhibitors. **(b)** Crystal structure of rkbPAP (yellow surface) in complex with compound **4a** (as sticks with cyan carbons), and **(c)** in complex with **2**.Water molecules are shown as red spheres [27].

Using compounds **2** and **4a** as starting points, we generated two series of derivatives (*i.e.* **7a-b** and **4b-h**, respectively). To synthesise the two monocyclic alkoxy benzyl ether derivatives (**7a-b**) of compound **2** (*i.e.* the benzofuran) the 2-alkoxy benzaldehydes (**6a-b**) were first prepared by alkylation of salicylaldehyde (**5**) using alkyl halides and potassium carbonate in DMF solution, followed by sodium borohydride reduction to the corresponding benzyl alcohols [34] (Scheme 1).

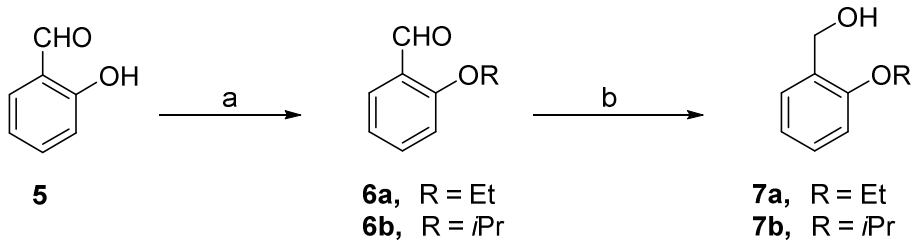

Scheme 1. Reagents and Conditions: (a) RX, K_2CO_3, DMF, r.t., 36 h. **6a** (86%), **6b** (84%); (b) $NaBH_4$, 2 M, NaOH, MeOH, r.t., 4 h. **7a** (74%); **7b** (85%).

The preparation of compounds **4a-f** first required the synthesis of the intermediates **11a-f**, as outlined in Scheme 2. Following the method described by Gududuru *et al.* [35], the hydrochloride salt of the methyl ester of L-cysteine (**9**), which was first prepared by refluxing L-cysteine (**8**) with $SOCl_2$ in methanol, was reacted with a series of aromatic aldehydes **10a-f** to give the corresponding thiazolidine methyl ester intermediates **11a-f**.

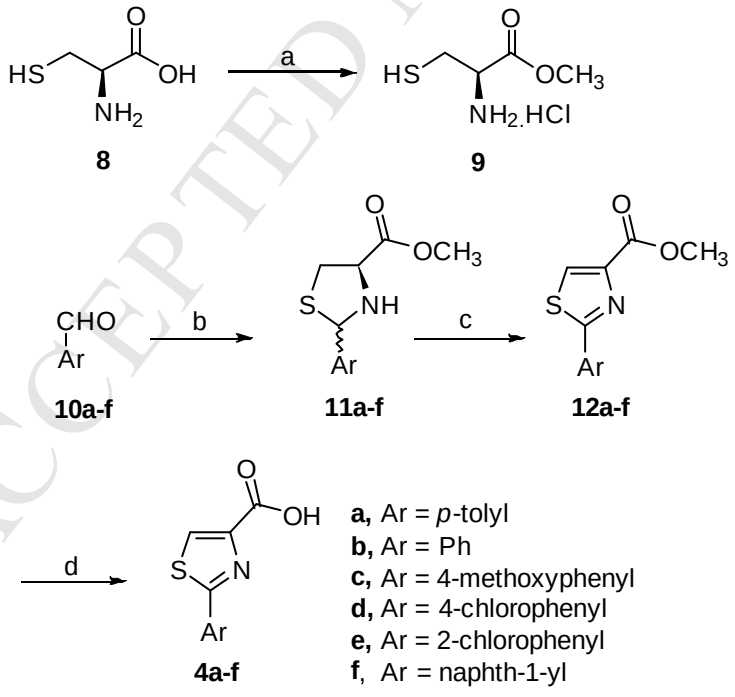

Scheme 2. Reagents and Conditions: (a) $SOCl_2$, MeOH, Δ, 3 h, 100%; (b) **9**, $NaHCO_3$, EtOH, H_2O, r.t., 14 h. **11a** (65%); **11b** (74%); **11c** (81%); **11d** (57%); **11e** (79%); **11f** (37%); (c) *N*-

bromosuccinimide, benzoyl peroxide, CCl_4, Δ, 14 h. **12a** (23%), **12b** (26%), **12c** (17%), **12d** (19%), **12e** (32%), **12f** (16%); (d) 2 M NaOH, MeOH, 0 ºC, 2 h. **4a** (98%), **4b** (80%), **4c** (84%), **4d** (100%), **4e** (100%), **4f** (100%).

The thiazole carboxylic acid derivatives **4a-f** were prepared in two steps from their corresponding thiazolidine intermediates **11a-f**, by oxidation of **11a-f** using *N*-bromosuccinimide (NBS) and benzoyl peroxide, followed by basic hydrolysis of the methyl esters **12a-f**, using the method described by Gududuru *et al.* [35] (Scheme 2).

The syntheses of the thiazole dicarboxylic acids **4g-h** are outlined in Scheme 3. Following the method described by Ashram [36], the two aromatic aldehydes **13** and **15** were prepared by refluxing the 2-hydroxy aromatic aldehydes **5** and **14**, respectively, with ethyl 2-bromoacetate in the presence of potassium carbonate in acetone. The two aromatic aldehydes, **13** and **15**, then reacted with compound **9** to give the corresponding thiazolidine derivatives **11g-h** in 12% and 77% yields, respectively. Oxidation of **11g-h** to the thiazoles **12g-h**, followed by saponification, gave the carboxylic acids **4g-h** [35] (Scheme 3).

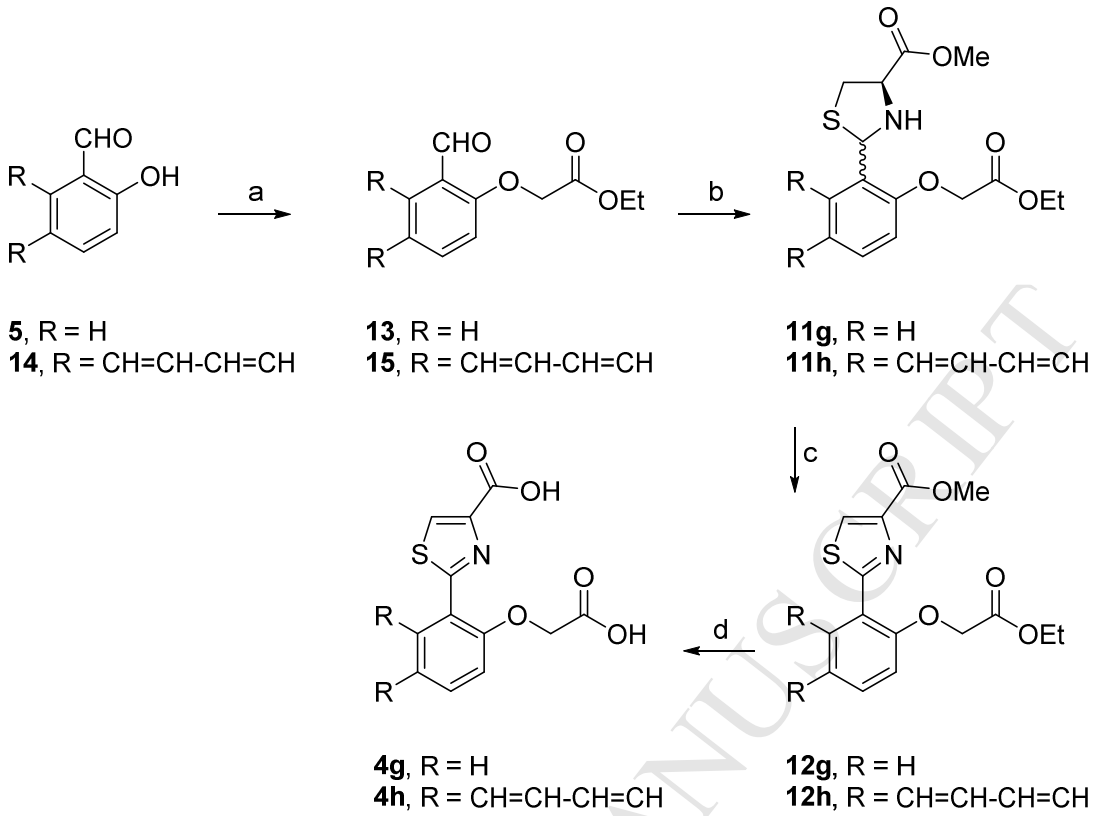

Scheme 3. Reagents and Conditions: (a) $BrCH_2CO_2Et$, K_2CO_3, Me_2CO, Δ, 4 h. **13** (86%), **15** (48%); (b) **9**, $NaHCO_3$, EtOH, H_2O, r.t., 14 h. **11g** (12%), **11h** (77%); (c) *N*-bromosuccinimide, benzoyl peroxide, CCl_4, Δ, 14 h. **12g** (17%), **12h** (8%); (d) 2 M NaOH, MeOH, r.t., 4 h. **4g** (73%), **4h** (80%).

Additionally, a series of thiazolidine-4-carboxylic acid derivatives **16a-c** and **16f-j** were synthesised for testing against both rkb and pig PAP enzymes to investigate the importance of the unsaturation of the thiazole ring for the activity of the compounds. Treating L-cysteine (**8**) with a number of aromatic aldehydes **10a-c** and **10f-j** in ethanol solution gave the corresponding thiazolidine-4-carboxylic acid derivatives **16a-c** and **16f-j**, as mixtures of *cis* and *trans* isomers, in good yields [35] (Scheme 4).

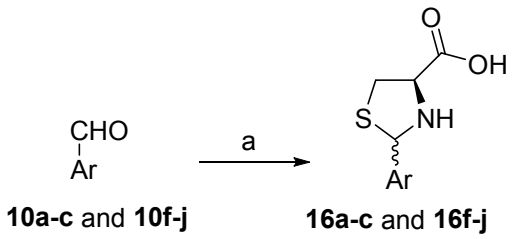

a, Ar = *p*-tolyl
b, Ar = Ph
c, Ar = 4-methoxyphenyl
f, Ar = naphth-1-yl
g, Ar = 2-hydroxynaphth-1-yl
h, Ar = 4-hydroxyphenyl
i, Ar = 2-hydroxyphenyl
j, Ar = 2-furyl

Scheme 4. Reagents and Conditions: (a) L-Cysteine (**8**), EtOH, r.t., 5 h. **16a** (63%), **16b** (66%), **16c** (52%), **16f** (68%), **16g** (70%), **16h** (64%), **16i** (93%), **16j** (66%).

Inhibition assays: The inhibitory effects of compounds **7a-b** and **4a-h** were tested using a standard kinetic assay with the chromophoric substrate *para*-nitrophenyl phosphate (*p*NPP); both rkbPAP and fully reduced pig PAP were used. In the first round of assessment, percentage inhibition was measured at a fixed concentration (*i.e.* 100 μM) of inhibitor. This initial screen indicated that compound **4f** was the most promising lead; both pig PAP and rkbPAP activities were reduced to approximately half the value measured in its absence. Since accurate measurement of the binding affinity of a possible inhibitor also depends on its mode of binding and its competition with a substrate of the reaction, several of the above compounds were tested in inhibition assays where the concentrations of both the substrate and inhibitors were varied. Relevant parameters are summarised in Table 1. K_{ic} and K_{iuc} represent the inhibitor dissociation constants for the enzyme-inhibitor and enzyme-substrate-inhibitor complex, respectively (*i.e.* competitive vs uncompetitive inhibition constants). Compounds 7**a-b** and **4g-h** exhibited little or no inhibitory activity against either pig or rkbPAP

Table 1: Kinetic data for inhibitors **4a-f** against fully reduced pig PAP and rkbPAP at pH 4.9.

Compound	Enzyme	K_{ic} (μM)	K_{iuc} (μM)
4a	Pig PAP	42 ± 14	-
4a	rkbPAP	340 ± 130	-
4b	Pig PAP	190 ± 62	-
4b	rkbPAP	-	-
4c	Pig PAP	120 ± 35	-
4c	rkbPAP	400 ± 210	770 ± 700
4d	Pig PAP	49 ± 13	-
4d	rkbPAP	530 ± 480	-
4e	Pig PAP	630 ± 570	350 ± 180
4e	rkbPAP	920 ± 630	-
4f	Pig PAP	33 ± 15	110 ± 69
4f	rkbPAP	185 ± 75	-

For each of the compounds **4a** – **4f** their inhibitory effects on pig PAP and rkbPAP are within the same order of magnitude, but in each case the binding is stronger for the pig enzyme, and in most cases the mode of inhibition is competitive. The exceptions are compounds **4e** and **4f** that also have a contribution from an uncompetitive binding mode (characterised by K_{iuc}) in pig PAP. However, overall only compound **4f** has a binding affinity (based on the magnitude of respective K_i values) that is modestly better than that of the parental compound **4a** (Table 1).

The thiazolidine-4-carboxylic acid derivatives **16a-c** and **16f-j** were tested against a fully reduced pig PAP enzyme at 100 μM concentrations using 5 mM *p*NPP as a substrate. This

series of compounds did not show any inhibition effect, except for compound **16k**, that displays modest (~40%) inhibition. Consequently, this series of compounds was not further investigated.

Crystallographic investigations of inhibitor binding

Crystallographic investigations into the binding mode of compound **4f** in complex with rkbPAP were undertaken wherein a rkbPAP crystal was grown and then soaked with a solution containing **4f**. The crystal diffracted to 2.4 Å resolution (Table 2) and has the same space group as described previously [27], and with the asymmetric unit consisting of two dimers of rkbPAP; the monomers are denoted A through D. After fitting of the polypeptide, amino acid side chains, metal ions and solvent molecules, **4f** was modelled into the difference electron densities of Polder omit maps. Polder maps were chosen for this study since they are optimal for visualisation of weak binding inhibitors obscured by bulk solvent scaling [37]. Compound **4f** was modelled in subunit A (> 4.75 σ) and subunit B (> 5.24 σ) (Figure 2A,B). In subunits C and D, the difference electron densities indicate the presence of a sulfate anion bound to the metal centre.

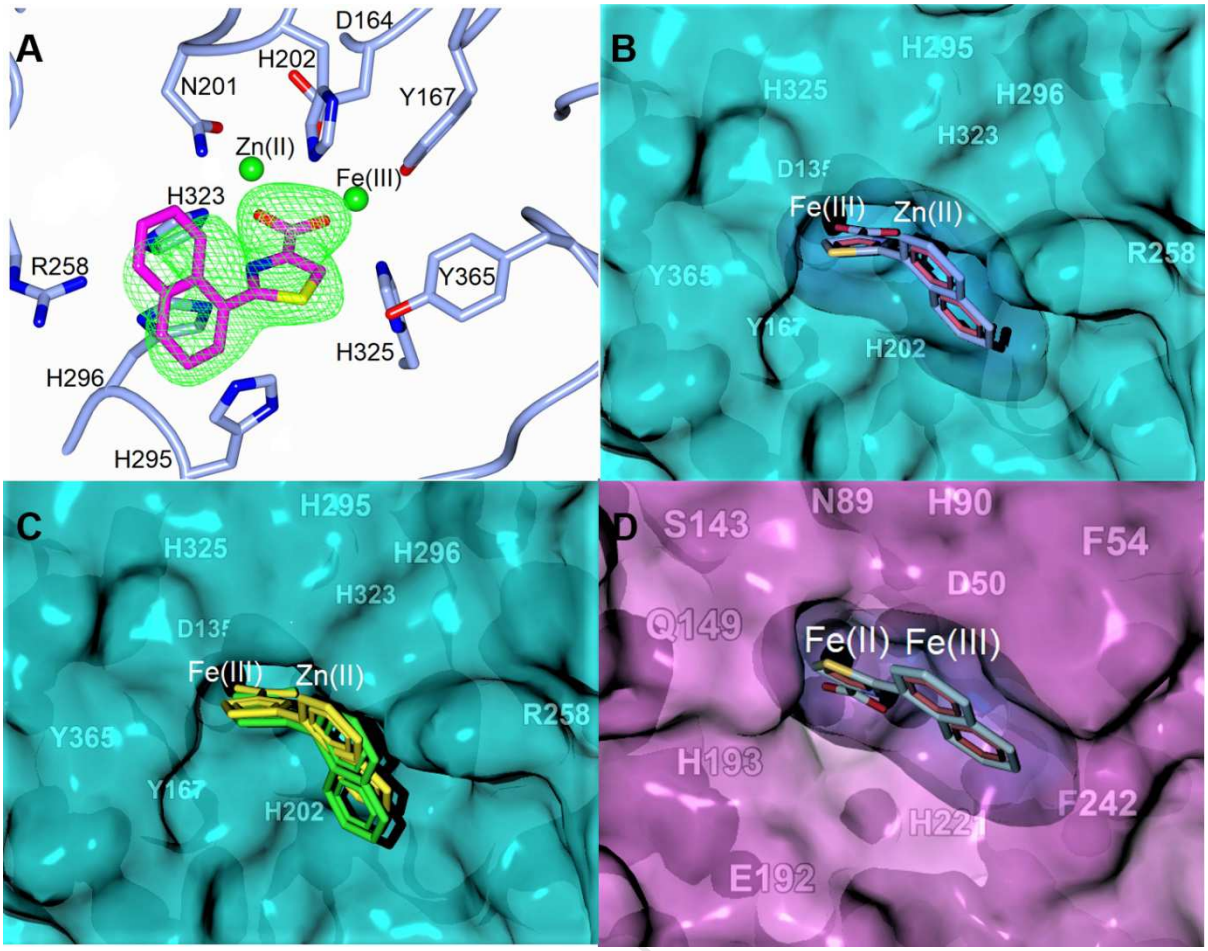

Figure 2: (A) Polder (Fo-Fc) omit electron density map (> 5.24 σ) and cartoon/stick representation showing the fit of the inhibitor **4f** (magenta carbons) to the difference electron density in subunit B of rkbPAP (light blue carbons), the metals are shown as green spheres (B) Surface and stick representation of the active site of rkbPAP (turquoise surface) in complex with **4f** (CPK colouring sticks and blue surface), metals are shown as black spheres. For clarity of presentation, this view is rotated by 180º relative to 2(A). (C) Surface and stick representation showing the result of MVD predicting the binding mode of **4f** (green sticks) to rkbPAP superimposed onto the crystal structure of rkbPAP (turquoise surface) in complex with **4f** (yellow sticks); the metals are shown as black spheres (D) Surface and stick representation showing the result of MVD predicting the binding mode of **4f** (CPK colouring sticks, blue surface) to human PAP (purple surface); the metals are shown as black spheres.

The inhibitor binds through its carboxylate group in a μ-1,3 bidentate mode to the metal ions in the active site, more closely to Fe(III) (1.7 Å) than to Zn(II) (2.2 Å) (Figure 2A). The sulfur atom in the thiazole ring of the inhibitor forms a hydrogen bond with the hydroxyl group of the adjacent Y365 side chain (3.2 Å). The nitrogen atom in the thiazole ring forms a hydrogen bond (3.0 Å) with a nitrogen atom in the imidazole group of H296, and the thiazole ring forms π-cation

interactions with H295 and H296 (3.0-4.0 Å). The naphthalene ring, while not as well resolved as the thiazole ring (likely to be due to some structural flexibility), forms π-cation interactions with the guanidino group of R258 from the adjacent subunit in the rkbPAP dimer (3.3-4.0 Å) and with the imidazole group of H295 (2.90-3.70 Å). In comparison to the binding interactions of compound **4a** (Figure 3) both the carboxylate and thiazole moieties are positioned similarly in the two molecules, suggesting that the naphthalene ring in **4f** enhances inhibitor binding despite not being locked in place by non-covalent associations. This indicates further improvements are possible to improve potency.

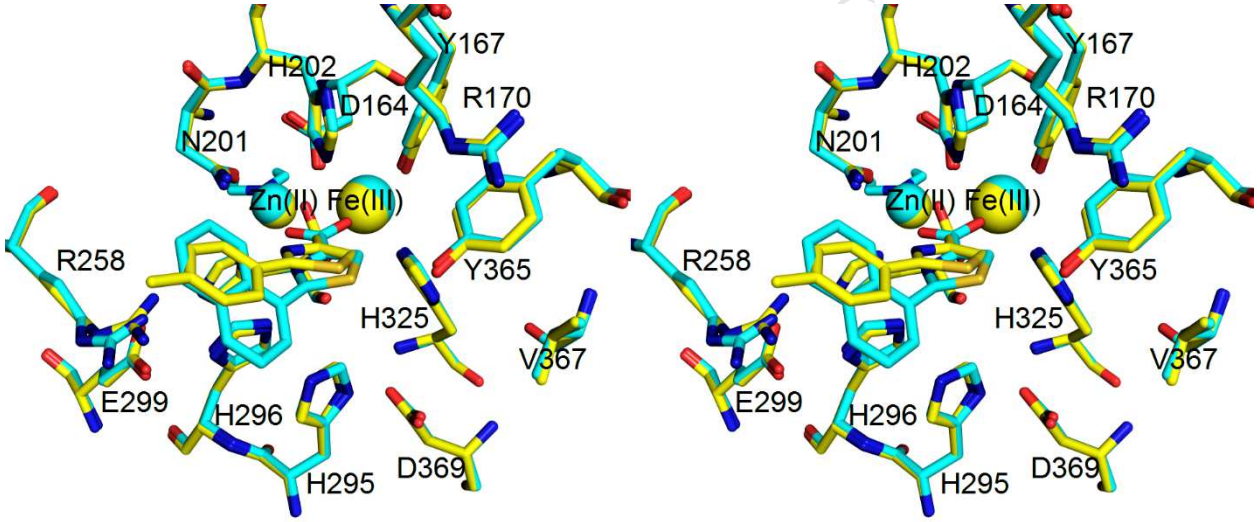

Figure 3: Stereo superimposition of the crystal structure of rkbPAP with **4a** bound to the active site of subunit B (PDB ID: 4DHL, yellow carbons) and rkbPAP with **4f** bound to the active site of subunit B (cyan carbons) to the active site. Substitution of the *p*-tolyl group with a *p*-naphthyl group picks up an additional interaction with H295.

Table 2: Data collection and refinement statistics for the rkbPAP-**4f** complex

Data collection	
Temperature	100
Resolution range (Å)	43.26 - 2.40 (2.49 - 2.40)[a]
Total number of reflections	467895 (30571)
Total number unique	107272 (10656)
Completeness (%)	99.4 (97.5)
$^{\wedge}R_{merge}$	0.083 (0.280)
Mean I/σI	10.9 (3.4)
CC(1/2)	0.98 (0.93)

Mosaicity (°)	0.27
Unit cell lengths (Å)	$a = b = 126.21$ $c = 297.12$
Space group	$P\,3_1\,2\,1$
Refinement	
Total number of atoms	15,764
Number of water molecules	1,225
Wilson B-factor (Å^2)	33.66
*R_{work}	0.172
#R_{free}	0.223
RMS bonds (Å)	0.009
RMS angles (°)	0.957
Ramachandran statistics (%)	
Favoured	95.02
Allowed	4.04
Outlier	0.94

*R_{work} = $\Sigma|F_o|-|F_c|/\Sigma|F_o|$ and is calculated using 95% of the total reflections, and #R_{free} uses the remaining 5% of the reflections. ^R_{merge} = $\Sigma_{hkl}\Sigma_i|I_i(hkl)-I(hkl)|/\Sigma_{hkl}\Sigma_i\ I_i(hkl)$. [a]Values in parentheses are for the highest resolution shell.

The occupancy and B-factors of the inhibitor and the neighbouring residues have been refined. The occupancy is close to 0.9 (0.84 on average) for the inhibitor and the B-factors for the inhibitor are, on average, approximately double that of the neighbouring residues (data not shown). This suggests that the inhibitor is stabilised in the active site but not necessarily bound with high affinity. The K_i value of 185 ± 75 for this compound with rkb PAP supports this.

Docking studies

Active site comparison of human, pig and red kidney bean PAPs

To further validate the use of red kidney bean PAP and pig PAP as model systems for human PAP, we carried out a three dimensional structure-based alignment. It shows that the position of the metal ions and the three-dimensional arrangement of the metal-coordinating residues are completely conserved across the three species and that the amino acids that form the surface of

the active site share 100% sequence identity between the human and pig enzymes (Figure 4). This makes pig PAP an ideal model for human PAP inhibitor design.

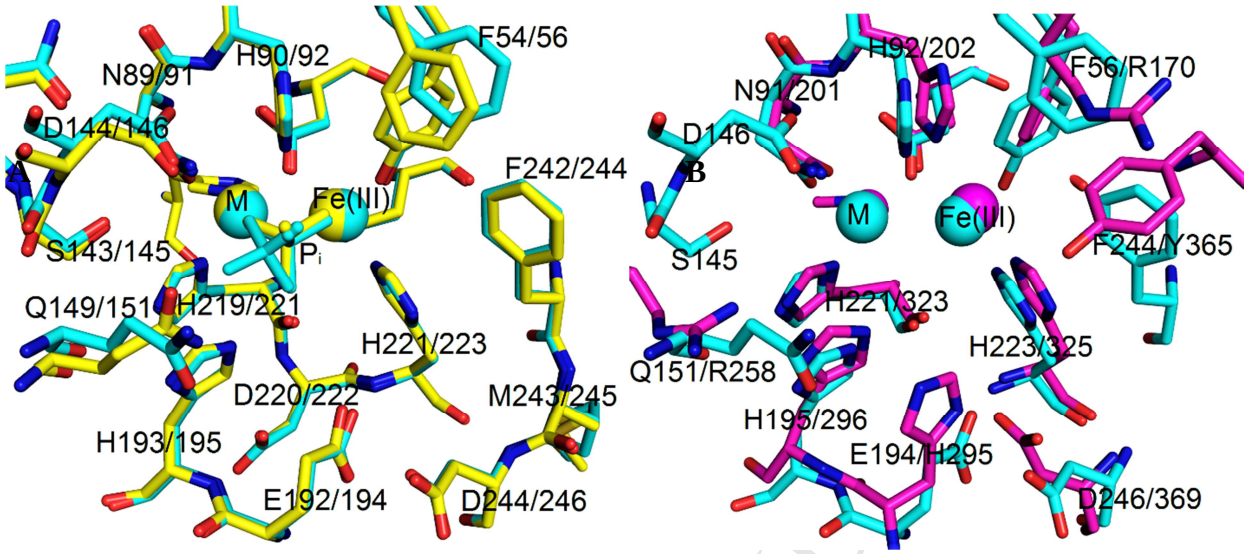

Figure 4: (A) Superimposition of the structure of pig PAP with two conformations of phosphate bound (PDB ID: 5UQ6, cyan) and recombinant human PAP with bound phosphate (PDB ID: 1WAR, yellow). All active site residues are fully conserved. (B) Structure-based alignment of the active sites of pig PAP (PDB ID: 5UQ6, cyan) and rkbPAP (PDB ID: 4KBP, magenta) with phosphate omitted, highlighting that most residues surrounding the active site are conserved or semi-conserved between the two enzymes. M is either Fe(II/III) in pig and human PAPs or Zn(II) in rkbPAP. P_i represents inorganic phosphate.

Docking studies were undertaken to predict the binding mode of **4f** to human PAP (Figure 2C-D). Firstly, the accuracy of the docking algorithm was gauged by verifying its ability to predict the correct binding mode of **4f** to rkbPAP. As seen previously [27], the MolDock Simplex Evolution (SE) algorithm can predict the correct binding mode of an inhibitor to rkbPAP with reasonable accuracy (Figure 2C). The same algorithm was used to dock **4f** to human PAP (Figure 2D). In the optimal conformation the carboxylate group of the inhibitor coordinates bidentately to the two metals in the active site as observed in the crystal structure of the rkbPAP-**4f** complex (Figure 2A). The thiazole ring of the inhibitor forms hydrophobic interactions with the side-chain of conserved N89 (N201 in rkbPAP). The thiazole sulfur is oriented towards a groove in the interface between the conserved metal ligating residues N89 and H221 (N201 and H325 in rkbPAP) and the mammalian repression loop (N142, S143 and D144, spatially equivalent Y365

in rkbPAP), whereby it is stabilised by van der Waals interactions with the side-chains of these residues and by a hydrogen bond with the side chain amino group of Q149. The remainder of the thiazole ring is stabilised by π-cation interactions with H90 and H193 (H202 and H296 in rkbPAP, respectively). The naphthalene ring fits into a hydrophobic wedge formed by the sidechains of F54 and F242. Pose binding energies obtained from Molegro Virtual Docker (MVD) algorithm are -89.51 kcal/mol and -56.61 kcal/mol for the interactions of **4f** with human PAP and rkbPAP, respectively, which suggests that this inhibitor binds tighter to the human enzyme, in good agreement with the enhanced affinity of **4f** for pig PAP when compared to rkbPAP (Table 1). The major contribution to the enhanced affinity of **4f** to the human enzyme is due to a stronger interaction of the naphthalene ring with the hydrophobic side chains of F54 and F242 when compared to R258 in rkbPAP; however, the thiazole portion of the inhibitor also contributes to the difference due to its interaction with the repression loop that is characteristic for mammalian PAPs.

3. Conclusion

The role of PAPs in bone resorption has been well established since studies of transgenic mice demonstrated that abnormal expression levels of this enzyme are associated with bone disorders; overexpression of PAP leads to an osteoporotic phenotype, while a knockout displays features characteristic of osteopetrosis [15]. While these observations make PAP a target for the development of chemotherapeutics to combat osteoporosis, little effort has been directed towards the design of specific and potent inhibitors of this enzyme. Though a recent paper used a small molecule screening library to identify a family of carboxamides as low micromolar inhibitors of human PAP [5], the majority of inhibitors discovered to date are simple anions (*e.g.* phosphate, vanadate or sulfate [1-4, 8-9, 19, 29] that target the bimetallic metal centre. Since the bimetallic metal centre and its seven amino acid ligands are well conserved amongst a range of metallohydrolases (as an example, enzymes such as the diesterases GpdQ and Rv0805 have an active site that is nearly identical to that of PAPs [38-39] it is not surprising that inhibitors targeting mainly the metal centre are non-specific. More complex molecules that may exploit structural features in the outer sphere of the PAP active site were developed but their precise binding modes had not been explored, largely due to the lack of crystallographic data. In this respect, the crystal structures of several small fragments in complex with rkbPAP provided, for the first time, detailed insight into how potential inhibitor leads may interact with a PAP [27]. Here, two of these fragments (**2** and **4a** in Figure 1a) were used as starting points for further elaboration. Of significance is that our structure activity relationship (SAR) results indicate that most of the thiazolidine derivatives of **16** are ineffective inhibitors of PAPs. The exception is compound **16k**, bearing a naphthalene ring. Upon oxidising its thiazolidine ring to the corresponding thiazole while retaining the naphthalene ring leads to compound **4f**. This compound displays improved

binding affinity, and its structure in complex with rkbPAP guides further modifications to enhance the binding specificity and potency (Figure 2).

To date it has not been possible to obtain crystal structures of catalytically active forms of a mammalian PAP. Available structures contain an inactive di-Fe(III) centre, mostly in complex with phosphate [40-41]. In contrast, plant PAPs crystallise readily in their catalytically active form, largely due to the fact that they contain redox-inactive Fe(III)Zn(II) or Fe(III)Mn(II) centres [8-11, 13, 42-43]. Consequently, in particular rkbPAP has been employed as a model to investigate the effect of inhibitors on PAPs. The observation of reasonably conserved (i) catalytic properties, including substrate specificities, mechanism and inhibition by non-specific inhibitors, and (ii) amino acid side chains in the vicinity of the active site validate the selection of rkbPAP as a model for mammalian PAPs [1-4]. Indeed, all compounds tested here have comparable inhibitory effects for pig PAP and rkbPAP, albeit their binding to the mammalian enzyme is always more potent (Table 1). In order to gain insight into how **4f** binds to the human enzyme *in silico* docking was employed. The methodology was initially tested using rkbPAP to demonstrate that the predicted (*in silico*) mode of binding of **4f** is virtually identical to that observed experimentally (in the crystal structure; Figure 2). Indeed, the inhibitor is predicted to bind better to the mammalian enzyme, in part due to additional interactions between this compound and the repression loop that is characteristic for mammalian PAPs [40]. This predicted improvement in binding is reflected in the lower K_i of pig PAP for **4f** when compared to rkbPAP (Table 1).

In summary, this study provides the first crystallographic insight into a rationally designed inhibitor for PAP. The structure provides guidance for the further elaboration of PAP inhibitors that may find applications in the treatment of conditions associated with elevated levels of this enzyme, including not only osteoporosis but potentially also AIDS

encephalopathy [44], Gaucher's disease [45], hairy cell leukemia [46], Alzheimer's disease [47] and bone metastases [48-49].

4. Experimental

4.1. Enzyme preparation and Purification

Purple acid phosphatase from red kidney bean (rkbPAP) was purified following a previously published protocol [50]. Briefly, red kidney beans (*Phaseolus vulgaris*) were ground in a Waring blender and suspended in 0.5 M sodium chloride. The suspension was filtered through a muslin cloth, followed by ethanol fractionation and ammonium sulfate precipitation and further purified by ion-exchange chromatography using a CM-cellulose column followed by gel filtration on a Sephadex S-300 column. The resulting preparation was concentrated to 23.8 mg⁄mL using a Millipore Amicon centrifugal concentrator and stored at 4 ºC in 0.5 M sodium chloride. Pig PAP was extracted from the uterine fluid of a pregnant sow and purified by ion-exchange chromatography using CM-cellulose followed by gel filtration on a Sephadex G-75 [51]. Purified pig PAP was concentrated to 8.1 mg⁄mL and stored at 20 ^{o}C in 100 mM acetate buffer at pH 4.9. Protein concentrations were determined by measuring the absorbance at 280 nm using extinction coefficients of 1.41 for a 1 mg⁄mL solution (28.6 µM) of pig PAP and 2.1 for a 1 mg⁄mL solution (9.1 µM) of rkbPAP. SDS-PAGE analysis showed that the enzymes were >95% pure.

4.2. Crystallisation, soaking and cryoprotection

Crystallisation of rkbPAP was achieved using previously determined conditions [42]. Once crystals had reached a size of ~0.1 mm in all three dimensions, an equivalent volume of cryoprotectant containing the inhibitor was added to the hanging drop. This solution consisted of 0.1 M sodium citrate pH 5.0, 0.1 M lithium chloride, 25% polyethylene glycol 3350, 20% isopropyl alcohol, 10% glycerol and 4 mM of **4f**. This was introduced 4 days before the data

collection. For cryoprotection, a crystal from the above preparation was soaked in cryoprotectant (containing the inhibitor) for 10 s before placing it in the cryostream (100 K).

4.3. Data collection & analysis

Data were collected using a FR-E X-ray generator (voltage: 45 kV, current: 45 mA) and recorded using a Raxis IV++ imaging plate at UQ. CuKα X-rays (wavelength: 1.54 Å) were used for these diffraction studies. The program Rigaku Crystal clear 2.0 [52] was used to integrate and scale reflections and Scala in CCP4 was used to scale and merge the data [53]. Initial protein model for refinements was that of the crystal structure of rkbPAP in complex with **4a** (PDB access code: 4DHL) with the inhibitor removed from the active site. Refinements and building of Polder maps were performed using PHENIX [54] and model building was undertaken using Coot [55]. Figure 2A was produced using CCP4MG [56] and Figures 2B-D were produced using MVD [57]. Coordinates and structure factors for the complex have been deposited in the Protein Data Bank with access code 6G46.

4.4. Computational docking studies

Docking studies were undertaken with MVD [57] using the MolDock SE algorithm with flexible residues using Tabu clustering and softened potentials. The ligand search space was confined to a 9 Å sphere originating from the metal centre of PAP. For rkbPAP, the receptor coordinates used were those of the crystal structure of the enzyme in complex with the inhibitor obtained here. For human PAP, the coordinates used were those of recombinant human PAP in complex with phosphate (PDB code 1WAR) [40] with the phosphate anion omitted from the active site. Water molecules were removed from all coordinate files prior to docking.

4.5. **Enzyme kinetics**

Inhibition assays with both pig PAP and rkbPAP were performed in 96 well 400 µL multi-titre plates using a UV/Vis multiplate spectrophotometer [29]. Prior to its use in kinetic assays pPAP was fully reduced to the heterovalent Fe(III)Fe(II) state to ascertain maximum activity by incubating it with 0.77 mM β-mercaptoethanol for ten minutes at 37 ^{o}C. Kinetic measurements were carried out at pH 4.9 (0.1 M acetate buffer in 25% DMSO) at 25 ^{o}C using *para*-nitrophenyl phosphate (*p*NPP) as substrate at different concentrations (1, 3, 5, 7.5, 10 and 12.5 mM). The rate of product (*p*-nitrophenol) formation was measured at λ = 405 nm (ε = 343 $M^{-1}cm^{-1}$) [13]. Enzyme concentration used was 12 nM, while the concentrations for tested compounds ranged from 50 µM to 300 µM. The data were analysed by non-linear regression using the general inhibition equation (equation 2) and the program WinCurveFit (Kevin Raner software).

$$v = \frac{V_{max}[S]}{[S]\left(1 + \frac{[I]}{K_{iuc}}\right) + K_M\left(1 + \frac{[I]}{K_{ic}}\right)}$$

Equation 2

In this equation, K_{ic} and K_{iuc} represent the equilibrium dissociation constants for competitive and uncompetitive inhibitor binding, respectively, while V_{max}, K_M, [S] and [I] represent the maximum rate of product formation, the Michaelis constant, substrate concentration and inhibitor concentration, respectively.

4.6. Experimental chemistry

Light petroleum (LP, b.p. 40-60 °C) was distilled before use. Flash chromatography was carried out with Merck Kieselgel 60 as described by Still [58]. NMR experiments were recorded on 300, 400 and 500 MHz spectrometers (Bruker, Rheinstetten, Germany). Chemical shifts are reported in parts per million (ppm) on a δ scale, relative to the solvent peak ($CDCl_3$ δ_H 7.24, δ_C 77.0; $(CD_3)_2SO$ δ_H 2.49, δ_C 39.5; MeOD δ_H 3.30, δ_C 49.0). Coupling

constants (*J*) are reported in hertz and peak multiplicities described as singlet (s), doublet (d), triplet (t), quartet (q), septet (sept), multiplet (m), or broad (br). High resolution electrospray ionisation accurate mass measurements were recorded in positive and negative mode on a quadrupole – time of flight instrument (Bruker) with an ESI source. Accurate mass measurements were carried out with external calibration using sodium formate as reference calibrant and/or Agilent tune mix (mw > 500). Low and high resolution electron impact ionisation mass measurements were recorded using perfluorokerosene-H as reference calibrant. For TLC staining, $Ce(SO_4)_2$ and/or $KMnO_4$ were used. $Ce(SO_4)_2$ dye ingredients: 2.5 g phosphomolybdic acid; 1 g ceric sulfate; 100 mL water and 8 mL concentrated sulfuric acid. $KMnO_4$ dye ingredients: 3 g potassium permanganate; 20 g potassium carbonate; 5 mL 5% sodium hydroxide and 300 mL water.

4.6.1. General method for preparation of 2-alkoxy benzaldehydes (6a-b) [59]

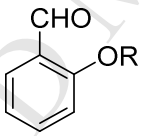

6a-b

Salicylaldehyde (**5**) (3.66 g, 3.2 mL, 30 mmol) was added to a suspension of potassium carbonate (8.29 g, 60 mmol) in DMF (50 mL). Alkyl halide was then added dropwise and the solution was stirred for 36 h under an atmosphere of argon. Water (150 mL) was added and the mixture was extracted with diethyl ether (3 x 50 mL). The combined organic layers were washed with 2M NaOH (3 x 50 mL), dried over Na_2SO_4, filtered and evaporated in vacuo to afford the 2-alkoxy benzaldehyde **6a-b**.

4.6.1.1. 2-Ethoxybenzaldehyde (6a) [59]

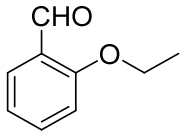

6a

The alkyl halide used was ethyl iodide (1 eq, 4.68 g, 2.4 mL, 30 mmol), which afforded **6a** as a yellow oil (3.85 g, 86%). R_f *:* 0.51 (10% EtOAc in LP, UV and $KMnO_4$ dip). ^{1}H NMR (300 MHz, $CDCl_3$) δ 1.38 (3H, t, *J* 7.0 Hz), 4.06 (2H, q, *J* 7.0 Hz), 6.87 – 6.93 (2H, m), 7.43 – 7.47 (1H, m), 7.71 (1H, dd, *J* 1.8 Hz, *J* 7.5 Hz), 10.41 (1H, s); ^{13}C NMR (75 MHz, $CDCl_3$) δ 14.4, 64.0, 112.4, 120.3, 124.6, 128.0, 135.8, 161.2, 189.8. NMR spectra are in agreement with those reported by Leardini [59].

4.6.1.2. 2-Isopropoxybenzaldehyde (6b) [59]

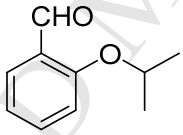

6b

The alkyl halide used was isopropyl bromide (1.1 eq, 4.06 g, 3.1 mL, 33 mmol), which afforded **6b** as a yellow oil (4.1 g, 84%). R_f *:* 0.59 (10% EtOAc in LP, UV and $KMnO_4$ dip). ^{1}H NMR (400 MHz, $CDCl_3$) δ 1.34 (6H, d, *J* 6.0 Hz), 4.62 (1H, sept, *J* 6.0 Hz), 6.90 – 6.95 (2H, m), 7.43 – 7.48 (1H, m), 7.77 (1H, dd, *J* 1.9 Hz, *J* 7.6 Hz), 10.45 (1H, s); ^{13}C NMR (100 MHz, $CDCl_3$) δ 21.8, 70.9, 113.9, 120.2, 125.6, 128.1, 135.6, 160.5, 190.0. NMR spectra are in agreement with those reported by Leardini [59].

4.6.2. General method for preparation of 2-alkoxy benzyl alcohols (7a-b)

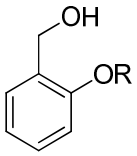

7a-b

These compounds **7a-b** were prepared using the general method described by Zartler and Sharpiro [34]. A solution of sodium borohydride (0.37 eq, 28 mg, 0.74 mmol) in 2M NaOH (40 µL) diluted with water (360 µL) was added dropwise to a solution of the 2-alkoxy benzaldehyde (**6a-b**) (2 mmol) in methanol (2 mL) at 18 – 25 ^{o}C. The reaction mixture was stirred for 4 h at room temperature and then evaporated in vacuo. Methanol (2 x 10 mL) was added and evaporated in vacuo. HCl (5%, 10 mL) was added to the residue which was extracted with diethyl ether (2 x 20 mL). The combined organic layers were dried over Na_2SO_4, filtered and evaporated in vacuo to afford **7a-b**.

4.6.2.1. 2-Ethoxybenzyl alcohol (7a)

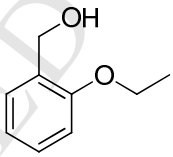

7a

The crude product was purified by silica flash column chromatography (10% EtOAc in LP) to afford **7a** as a colourless oil (224 mg, 74%) R_f *:* 0.28 (10% EtOAc in LP, UV and $KMnO_4$ dip). ^{1}H NMR (300 MHz, $CDCl_3$) δ 1.41 (3H, t, *J* 7.0 Hz), 3.18 (1H, s, OH), 4.02 (2H, q, *J* 7.0 Hz), 4.68 (2H, s), 6.83 (1H, d, *J* 8.2 Hz), 6.92 (1H, dt, *J* 0.8 Hz, *J* 7.4 Hz), 7.21 – 7.32 (2H, m); ^{13}C NMR (75 MHz, $CDCl_3$) δ 14.5, 61.0, 63.2, 110.7, 120.1, 128.0, 128.2, 129.1, 156.2. NMR spectra are in agreement with those reported by Wang [60].

4.6.2.2. 2-Isopropoxybenzyl alcohol (7b)

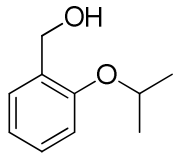

7b

Colorless oil (282 mg, 85%) R_f *:* 0.43 (10% EtOAc in LP, UV and $KMnO_4$ dip). ^{1}H NMR (500 MHz, $CDCl_3$) δ 1.36 (6H, d, *J* 6.1 Hz), 2.92 (1H, br s, OH), 4.61 (1H, sept, *J* 6.2 Hz), 4.67 (2H, s), 6.89 (1H, d, *J* 8.3 Hz), 6.92 (1H, dt, *J* 0.9 Hz, *J* 7.4 Hz), 7.23 – 7.29 (2H, m) in agreement with that reported by Fukatsu *et al.* [61]; ^{13}C NMR (125 MHz, $CDCl_3$) δ 22.0, 62.0, 70.0, 112.4, 120.3, 128.5, 128.6, 130.0, 155.6.

4.6.3. General method for preparation of 2-aryl-1,3-thiazolidine methyl esters (11a-f)

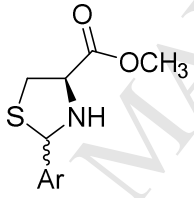

11a-f

These compounds **11a-f** were prepared using the general method described by Gududuru *et al.* [35].

Thionyl chloride (8.3 mL, 110 mmol) was added dropwise under an atmosphere of argon to a solution of L-cysteine (**8**) (9.00 g, 74 mmol) in 150 mL MeOH. The reaction mixture was refluxed for 3 h then evaporated in vacuo, then co-evaporated with toluene (2 x 5 mL) to afford the hydrochloride salt of the methyl ester of L-cysteine (**9**) as white solid. One-sixth of this material (**9**) (12.4 mmol) was dissolved in water/ ethanol (1:1) (15 mL). Sodium hydrogen carbonate (1.14 g, 13.6 mmol) was added and, after 10 min, the aromatic aldehyde (**10a-f**) (12.38 mmol) was added and the reaction mixture was stirred for 14 h. The ethanol was evaporated in vacuo and the aqueous residue was extracted with DCM (50 mL). The

organic layer was washed with water (25 mL), dried over Na_2SO_4, filtered and evaporated in vacuo to afford the crude products **11a-f**.

4.6.3.1. (2*R*/2*S*, 4*R*)-Methyl 2-(*p*-tolyl)thiazolidine-4-carboxylate (11a)

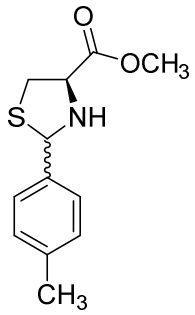

11a

The crude product was purified by silica flash column chromatography (10% EtOAc in LP) to afford a mixture of *cis* and *trans* isomers of **11a** as a yellow oil (1.90 g, 65%) R_f*:* 0.31 (20% EtOAc in LP, UV and $Ce(SO_4)_2$ dip). ^{1}H NMR (300 MHz, $CDCl_3$) δ 2.32 (s) and 2.34 (s) integrate for 3H, 2.72 (1H, br s, NH), 3.06 – 3.21 (1H, m), 3.32 – 3.52 (1H, m), 3.77 (s) and 3.76 (s) integrate for 3H, 3.96 (0.6H, dd, *J* 7.1 Hz, *J* 8.9 Hz), 4.21 (0.4H, dd, *J* 5.7 Hz, *J* 7.1 Hz), 5.52 (0.6H, s), 5.77 (0.4H, s), 7.11 – 7.17 (2H, m), 7.35 – 7.42 (2H, m); ^{13}C NMR (75 MHz, $CDCl_3$) δ 20.8, 20.9, 37.8, 38.9, 52.16, 52.22, 64.1, 65.2, 70.5, 72.2, 126.6, 127.0, 128.8, 129.0, 134.9, 137.3, 137.8, 138.2, 171.3, 171.9 in agreement with that described by Paul and Korytnyk [62].

4.6.3.2. (2*R*/2*S*, 4*R*)-Methyl 2-phenylthiazolidine-4-carboxylate (11b) [35]

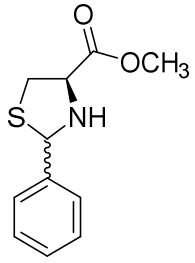

11b

The crude product was purified by silica flash column chromatography (10% EtOAc in LP) to afford *cis* and *trans* mixture of **11b** as a yellow oil (2.055 g, 74%) R_f *:* 0.31 (20% EtOAc in LP, UV and $Ce(SO_4)_2$ dip). ^{1}H NMR (300 MHz, $CDCl_3$) δ 2.65 (1H, br s, NH), 3.11 (1H, dd, *J* 9.0 Hz, *J* 10.2 Hz), 3.20 (0.5H, dd, *J* 6.0 Hz, *J* 10.8 Hz), 3.38 (0.5H, t, *J* 10.5 Hz), 3.41 – 3.49 (1H, m), 3.79 (1.5H, s), 3.80 (3H, s), 3.99 (1H, dd, *J* 7.2 Hz, *J* 9.0 Hz), 4.21 (0.5H, dd, *J* 6.0 Hz, *J* 6.9 Hz), 5.56 (1H, s), 5.82 (0.5H, s), 7.23 – 7.40 (5H, m), 7.47 – 7.52 (3H, m) in agreement with that described by Gududuru *et al.* [35]; ^{13}C NMR (75 MHz, $CDCl_3$) δ 38.0, 39.1, 52.4, 52.5, 64.2, 65.4, 70.7, 72.5, 126.8, 127.3, 127.8, 128.3, 128.57, 128.60, 138.1, 141.0, 171.5, 172.1.

4.6.3.3. (2*R*/2*S*, 4*R*)-Methyl 2-(4-methoxyphenyl)thiazolidine-4-carboxylate (11c)

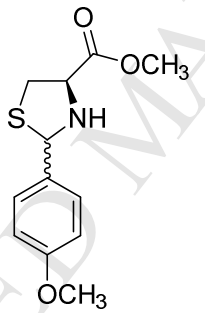

11c

The crude product was purified by silica flash column chromatography (10-60% EtOAc in LP) to afford *cis* and *trans* mixture of **11c** as a yellow oil (2.525 g, 81%) R_f *:* 0.19 (20% EtOAc in LP, UV and $Ce(SO_4)_2$ dip). ESI – MS, m/z: 276 $[M + Na]^+$. HRMS calculated for $C_{12}H_{15}NNaO_3S^+$ 276.0665, found 296.0654. ^{1}H NMR (500 MHz, $CDCl_3$) δ 3.08 (dd, *J* 8.9 Hz, *J* 10.3 Hz) and 3.20 (dd, *J* 5.5 Hz, *J* 10.7 Hz) integrate for 1H, 3.36 (dd, *J* 7.1 Hz, *J* 10.7 Hz) and 3.43 (dd, *J* 7.1 Hz, *J* 10.3 Hz) integrate for 1H, 3.766 (s), 3.770 (s), 3.78 (s) and 3.79 (s) integrate for 6H (2 x CH_3), 3.95 (0.7H, dd, *J* 7.2 Hz, *J* 9.0), 4.21 (0.3H, dd, *J* 5.5 Hz, *J* 7.2 Hz), 5.50 (s) and 5.74 (s) integrate for 1H, 6.83 – 6.88 (2H, m), 7.38 – 7.44 (2H, m); ^{13}C NMR (125 MHz, $CDCl_3$) δ 38.0, 39.2, 52.5, 52.6, 55.27, 55.29, 64.2, 65.4, 70.6, 72.3, 113.7,

114.0, 128.2, 128.7, 130.1, 132.9, 159.3, 159.8, 171.6, 172.3. NMR spectra are in agreement with those reported by Anwar and Moloney [63].

4.6.3.4. (2*R*/2*S*, 4*R*)-Methyl 2-(4-chlorophenyl)thiazolidine-4-carboxylate (11d)

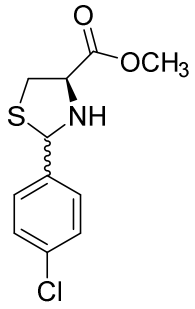

11d

The crude product was purified by silica flash column chromatography (10-50% EtOAc in LP) to afford *cis* and *trans* mixture of **11d** as a yellow oil (1.80 g, 57%) R_f*:* 0.31 (20% EtOAc in LP, UV and $Ce(SO_4)_2$ dip). ESI – MS, m/z: 280 $[M + Na]^+$. HRMS calculated for $C_{11}H_{12}ClNNaO_2S^+$ 280.0169, found 280.0171. ^{1}H NMR (300 MHz, $CDCl_3$) δ 2.68 (1H, br s, NH), 3.06 – 3.18 (1H, m), 3.35 (dd, *J* 7.1 Hz, *J* 10.6 Hz) and 3.44 (dd, *J* 7.1 Hz, *J* 10.3 Hz) integrate for 1H, 3.78 (s) and 3.79 (s) integrate for 3H, 3.96 (0.6H, dd, *J* 7.1 Hz, *J* 8.9), 4.13 (0.4H, t, *J* 6.5 Hz), 5.54 (s) and 5.77 (s) integrate for 1H, 7.26 – 7.34 (2H, m), 7.40 – 7.47 (2H, m); ^{13}C NMR (75 MHz, $CDCl_3$) δ 38.0, 39.1, 52.48, 52.52, 64.0, 65.4, 69.8, 71.7, 128.2, 128.4, 128.7, 128.8, 133.4, 134.3, 136.7, 139.9, 171.4, 172.0.

4.6.3.5. (2*R*/2*S*, 4*R*)-Methyl 2-(2-chlorophenyl)thiazolidine-4-carboxylate (11e)

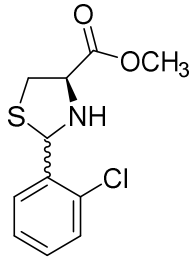

11e

The crude product was purified by silica flash column chromatography (10-50% EtOAc in LP) to afford *cis* and *trans* mixture of **11e** as a yellow oil (2.50 g, 79%) R_f*:* 0.37 (20% EtOAc in LP, UV and $Ce(SO_4)_2$ dip ESI – MS, m/z: 280 $[M + Na]^+$. HRMS calculated for $C_{11}H_{12}ClNNaO_2S^+$ 280.0169, found 280.0174. ^{1}H NMR (300 MHz, $CDCl_3$) δ 2.88 (1H, t, *J* 10.4 Hz, NH), 3.03 – 3.14 (1H, m), 3.33 (dd, *J* 6.5 Hz, *J* 10.6 Hz) and 3.46 (dd, *J* 6.9 Hz, *J* 10.2 Hz) integrate for 1H, 3.80 (s) and 3.81 (s) integrate for 3H, 3.99 (dd, *J* 4.0 Hz, *J* 6.9) and 4.25 (t, *J* 6.7 Hz) integrate for 1H, 5.94 (s) and 6.08 (s) integrate for 1H, 7.15 – 7.40 (4H, m), 7.57 (dd, *J* 1.7 Hz, *J* 7.6 Hz) and 7.71 (dd, *J* 2.1 Hz, *J* 7.5 Hz) integrate for 1H; ^{13}C NMR (75 MHz, $CDCl_3$) δ 37.4, 38.9, 52.5, 52.6, 65.4, 68.3, 126.5, 126.8, 127.3, 128.1, 128.5, 129.7, 129.8, 132.9, 133.7, 135.8, 140.0, 171.5, 172.0.

4.6.3.6. (2*R*/2*S*, 4*R*)-Methyl 2-(naphth-1-yl)thiazolidine-4-carboxylate (11f)

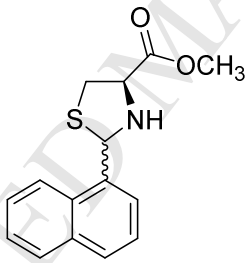

11f

The crude product was purified by recrystallisation from diethyl ether to afford *cis* and *trans* mixture of **11f** as white needles (1.232 g, 37%) R_f *:* 0.33 (20% EtOAc in LP, UV and $Ce(SO_4)_2$ dip). ESI – MS, m/z: 296 $[M + Na]^+$. HRMS calculated for $C_{15}H_{15}NNaO_2S^+$ 296.0716, found 296.0724. ^{1}H NMR (300 MHz, $CDCl_3$) δ 2.85 (1H, br s, NH), 3.12 (dd, *J* 9.3 Hz, *J* 10.2 Hz) and 3.20 (dd, *J* 6.3 Hz, *J* 10.5 Hz) integrate for 1H, 3.39 (dd, *J* 6.6 Hz, *J* 10.5 Hz) and 3.51 (dd, *J* 7.2 Hz, *J* 10.5 Hz) integrate for 1H, 3.80 (s) and 3.82 (s) integrate for 3H, 4.13 (dd, *J* 7.2 Hz, *J* 9.3 Hz) and 4.36 (t, *J* 6.5 Hz) integrate for 1H, 6.30 (s) and 6.49 (s) integrate for 1H, 7.40 – 7.58 (3H, m), 7.75 – 7.97 (3H, m), 8.13 (d, *J* 8.4) and 8.20 (d, *J* 8.4) integrate for 1H; ^{13}C NMR (75 MHz, $CDCl_3$) δ 37.9, 38.7, 52.6, 64.7, 65.6, 67.9, 69.3, 122.5,

123.5, 123.6, 123.8, 125.2, 125.3, 125.8, 125.9, 126.3, 126.5, 128.5, 128.7, 128.8, 129.2, 130.8, 131.4, 133.6, 133.7, 133.9, 136.6, 171.6, 172.3.

4.6.4. General method for preparation of 2-aryl-1,3-thiazole methyl esters (12a-f)

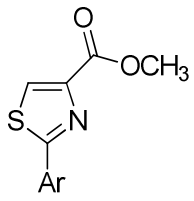

12a-f

These compounds **12a-f** were prepared using the general method described by Gududuru *et al.* [35]. NBS (2.1 eq, 835 mg, 4.69 mmol) and benzoyl peroxide (0.03 eq, 16.2 mg, 0.067 mmol) were added to a solution of **11a-f** (2.233 mmol) in CCl_4 (25 mL). The reaction mixture was refluxed for 14 h. The hot mixture was filtered and evaporated in vacuo. The crude product was purified by silica flash column chromatography to afford the corresponding thiazole derivatives **12a-f**.

4.6.4.1. Methyl 2-*p*-tolylthiazole-4-carboxylate (12a)

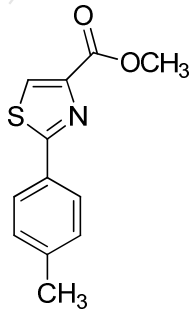

12a

The crude product was purified by silica flash column chromatography (0-10% EtOAc in LP) to afford **12a** as yellow solid (120 mg, 23%) R_f *:* 0.23 (10% EtOAc in LP, UV). ESI – MS, m/z: 256 $[M + Na]^+$. HRMS calculated for $C_{12}H_{11}NNaO_2S^+$ 256.0403, found 256.0404. ^1H NMR (300 MHz, $CDCl_3$) δ 2.35 (3H, s), 3.93 (3H, s), 7.19 (2H, d, *J* 8.0 Hz), 7.84 (2H, d, *J*

8.1 Hz), 8.10 (1H, s); ^{13}C NMR (75 MHz, $CDCl_3$) δ 21.4, 52.4, 126.8, 126.9, 129.6, 130.0, 141.0, 147.4, 161.9, 169.1. NMR spectra are in agreement with those reported by Wang *et al.* [64].

4.6.4.2. Methyl 2-phenylthiazole-4-carboxylate (12b)

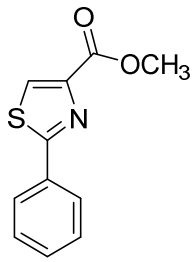

12b

The crude product was purified by silica flash column chromatography (0-10% EtOAc in LP) to afford **12b** as a yellow solid (139 mg, 26%) R_f*:* 0.23 (10% EtOAc in LP, UV and $KMnO_4$ dip). ^{1}H NMR (300 MHz, $CDCl_3$) δ 3.93 (3H, s), 7.39 – 7.41 (3H, m), 7.93 – 7.97 (2H, m), 8.12 (1H, s) in agreement with that described by Dawsey *et al.* [65]; ^{13}C NMR (75 MHz, $CDCl_3$) δ 52.3, 126.8, 127.2, 128.9, 130.6, 132.6, 147.6, 161.8, 168.9.

4.6.4.3. Methyl 2-(4-methoxyphenyl)thiazole-4-carboxylate (12c)

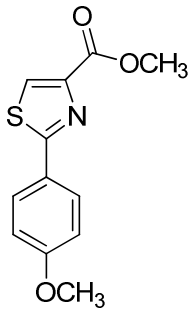

12c

The crude product was purified by silica flash column chromatography (0-60% EtOAc in LP) to afford **12c** as yellow solid (93 mg, 17%) R_f*:* 0.39 (20% EtOAc in LP, UV). ESI – MS, m/z: 272 $[M + Na]^+$. HRMS calculated for $C_{12}H_{11}NNaO_3S^+$ 272.0352, found 272.0352. ^{1}H NMR

(300 MHz, $CDCl_3$) δ 3.82 (3H, s), 3.93 (3H, s), 6.92 (2H, d, *J* 8.9 Hz), 7.89 (2H, d, *J* 8.9 Hz), 8.07 (1H, s); ^{13}C NMR (75 MHz, $CDCl_3$) δ 52.4, 55.4, 114.2, 126.5, 128.5, 131.7, 147.4, 161.6, 162.0, 168.8. NMR spectra are in agreement with those reported by Dawsey *et al.* [65].

4.6.4.4. Methyl 2-(4-chlorophenyl)thiazole-4-carboxylate (12d)

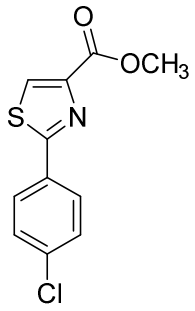

12d

The crude product was purified by silica flash column chromatography (0-10% EtOAc in LP) to afford **12d** as yellow solid (108 mg, 19%) R_f *:* 0.48 (20% EtOAc in LP, UV and $KMnO_4$ dip). ESI – MS, m/z: 276 $[M + Na]^+$. HRMS calculated for $C_{11}H_8ClNNaO_2S^+$ 275.9856, found 275.9860. ^1H NMR (300 MHz, $CDCl_3$) δ 3.93 (3H, s), 7.37 (2H, d, *J* 8.4 Hz), 7.88 (2H, d, *J* 8.5 Hz), 8.13 (1H, s); ^{13}C NMR (75 MHz, $CDCl_3$) δ 52.4, 127.4, 128.1, 129.2, 131.1, 136.7, 147.7, 161.7, 167.5.

4.6.4.5. Methyl 2-(2-chlorophenyl)thiazole-4-carboxylate (12e)

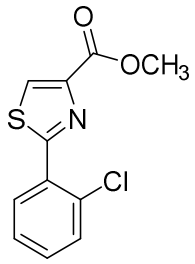

12e

The crude product was purified by silica flash column chromatography (0-10% EtOAc in LP) to afford **12e** as yellow solid (181 mg, 32%) R_f *:* 0.48 (20% EtOAc in LP, UV and $KMnO_4$

dip). ESI – MS, m/z: 276 $[M + Na]^+$. HRMS calculated for $C_{11}H_8ClNNaO_2S^+$ 275.9856, found 275.9859. ^{1}H NMR (300 MHz, $CDCl_3$) δ 3.90 (3H, s), 7.27 – 7.32 (2H, m), 7.39 – 7.42 (1H, m), 8.18 – 8.22 (1H, m), 8.23 (1H, s); ^{13}C NMR (75 MHz, $CDCl_3$) δ 52.3, 127.0, 128.6, 130.3, 130.8, 130.9, 131.2, 131.8, 146.1, 161.7, 164.0

4.6.4.6. Methyl 2-(naphth-1-yl)thiazole-4-carboxylate (12f)

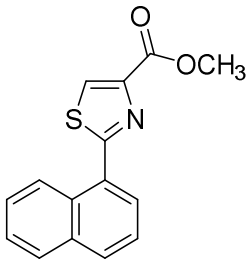

12f

The crude product was purified by silica flash column chromatography (0-10% EtOAc in LP) to afford **12f** as viscous yellow oil (95 mg, 16%) R_f *:* 0.42 (20% EtOAc in LP, UV and $KMnO_4$ dip). ESI – MS, m/z: 292 $[M + Na]^+$. HRMS calculated for $C_{15}H_{11}NNaO_2S^+$ 292.0403, found 292.0410. ^{1}H NMR (300 MHz, $CDCl_3$) δ 3.98 (3H, s), 7.47 – 7.63 (3H, m), 7.78 (1H, dd, *J* 1.2 Hz, *J* 7.2 Hz), 7.87 – 7.96 (2H, m), 8.30 (1H, s), 8.65 – 8.69 (1H, m); ^{13}C NMR (75 MHz, $CDCl_3$) δ 52.4, 124.9, 125.5, 126.5, 127.7, 128.2, 128.3, 128.8, 130.0, 130.5, 131.0, 133.8, 147.5, 162.0, 168.1. NMR spectra are in agreement with those reported by Liu *et al.* [66].

4.6.5. General method for preparation of 2-aryl-1,3-thiazole-4-carboxylic acids (4a-f)

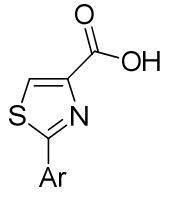

4a-f

These compounds **4a-f** were prepared using the general method described by Gududuru *et al.* [35]. Sodium hydroxide solution (1M, 2.5 mL) was added to a solution of (**12a-f**), 40-175 mg, in methanol (2.5 mL) at 0 ^{o}C. The solution was stirred for 2 h, and then the methanol was evaporated in vacuo. The solution was acidified with conc HCl and extracted with EtOAc (3 x 50 mL). The combined organic layers were washed with water (50 mL) and brine (50 mL), then dried over Na_2SO_4, filtered and evaporated in vacuo to afford the corresponding carboxylic acid derivatives **4a-f**.

4.6.5.1. 2-(*p*-Tolyl)thiazole-4-carboxylic acid (4a)

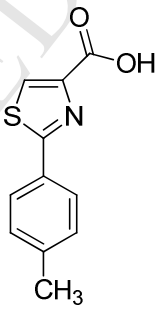

4a

4a was obtained as a white solid (39 mg, 98%) R_f *:* 0.12 (30% EtOAc in LP and 2 drops AcOH, UV and $KMnO_4$ dip). ^{1}H NMR (400 MHz, MeOD) δ 2.36 (3H, s), 7.26 (2H, d, *J* 7.6 Hz), 7.84 (2H, d, *J* 8.0 Hz), 8.27 (1H, s) in agreement with that reported by Aliabadi *et al.* [67]; ^{13}C NMR (100 MHz, MeOD) δ 21.4, 127.8, 128.5, 130.8, 131.4, 142.6, 149.2, 164.2, 170.6.

4.6.5.2. 2-Phenylthiazole-4-carboxylic acid (4b)

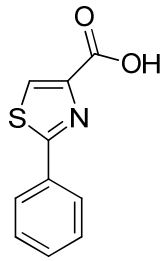

4b

4b was obtained as a white solid (77 mg, 80%) R_f *:* 0.10 (30% EtOAc in LP and 2 drops AcOH, UV and $KMnO_4$ dip). ^{1}H NMR (300 MHz, MeOD) δ 7.44 – 7.46 (3H, m), 7.95 – 7.98 (2H, m), 8.31 (1H, s) in agreement with that described by Zhao *et al.* [68]; ^{13}C NMR (75 MHz, MeOD) δ 127.8, 129.0, 130.2, 131.9, 134.0, 149.3, 164.1, 170.4.

4.6.5.3. 2-(4-Methoxyphenyl)thiazole-4-carboxylic acid (4c) [69]

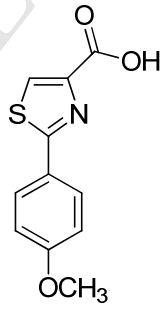

4c

4c was obtained as a yellow solid (58 mg, 84%). ^{1}H NMR (400 MHz, DMSO-d6) δ 3.82 (3H, s), 7.06 (2H, d, *J* 8.9 Hz), 7.90 (2H, d, *J* 8.9 Hz), 8.40 (1H, s); ^{13}C NMR (100 MHz, DMSO-d6) δ 55.4, 114.6, 127.8, 128.0, 130.4, 147.8, 161.2, 162.0, 167.3.

4.6.5.4. 2-(4-Chlorophenyl)thiazole-4-carboxylic acid (4d)

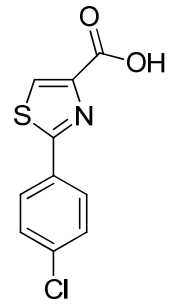

4d

4d was obtained as a white solid (101 mg, 100%). ^{1}H NMR (400 MHz, DMSO-d6) δ 7.58 (2H, d, *J* 8.5 Hz), 7.98 (2H, d, *J* 8.5 Hz), 8.51 (1H, s); ^{13}C NMR (100 MHz, DMSO-d6) δ 128.1, 129.2, 129.4, 131.3, 135.3, 148.2, 161.9, 166.1. NMR spectra are in agreement with those reported by Ma *et al.* [70].

4.6.5.5. 2-(2-Chlorophenyl)thiazole-4-carboxylic acid (4e)

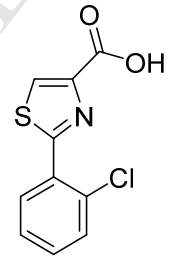

4e

4e was obtained as a white solid (165 mg, 100%). ^{1}H NMR (400 MHz, DMSO-d6) δ 7.50 – 7.57 (2H, m), 7.64 – 7.68 (1H, m), 8.16 – 8.20 (1H, m), 8.63 (1H, s) in agreement with that described by Carpenter *et al.* [71]; ^{13}C NMR (100 MHz, DMSO-d6) δ 127.9, 130.1, 130.7, 130.89, 130.90, 131.7, 147.0, 162.0, 162.7, 162.9.

4.6.5.6. 2-(Naphth-1-yl)thiazole-4-carboxylic acid (4f)

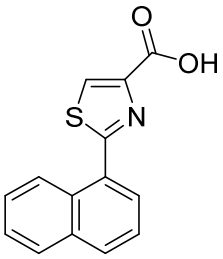

4f

4f was obtained as a white solid (88 mg, 100%). ^{1}H NMR (400 MHz, DMSO-d6) δ 7.60 – 7.68 (3H, m), 7.94 (1H, dd, *J* 1.2 Hz, *J* 7.2 Hz), 8.04 (1H, dd, *J* 1.7 Hz, *J* 7.7 Hz), 8.11 (1H, d, *J* 8.4 Hz), 8.63 (1H, s), 8.83 (1H, dd, *J* 0.9 Hz, *J* 8.1 Hz) in agreement with that described by Carpenter *et al.* [71]; ^{13}C NMR (100 MHz, DMSO-d6) δ 125.3, 125.4, 126.7, 127.7, 128.5, 128.9, 129.3, 129.45, 129.47, 131.0, 133.6, 148.1, 162.2, 166.9.

4.6.6. Synthesis of ethyl 2-(2-formylphenoxy)acetate (13) [36]

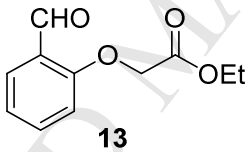

13

Salicylaldehyde (**5**) (2.50 g, 2.18 mL, 21 mmol) was added to a suspension of potassium carbonate (3.06 g, 22 mmol) in acetone (75 mL). The mixture was stirred for 5 min at room temperature under an argon atmosphere. Ethyl 2-bromoacetate (3.75 g, 2.49 mL, 23 mmol) was added to the reaction mixture and the mixture was refluxed for 4 h. After cooling, the reaction mixture was filtered and the residue was washed with acetone. The filtrate was evaporated in vacuo and the residue was dried under high vacuum to remove any traces of salicylaldehyde to give compound **13** (3.66 g, 86%) R_f *:* 0.21 (10% EtOAc in LP, UV and $KMnO_4$ dip). ^{1}H NMR (300 MHz, $CDCl_3$) δ 1.25 (3H, t, *J* 7.2 Hz), 4.23 (2H, q, *J* 7.1 Hz), 4.72 (2H, s), 6.83 (1H, d, *J* 8.4 Hz), 7.01 – 7.07 (1H, m), 7.46 – 7.52 (1H, m), 7.82 (1H, dd, *J* 1.8 Hz, *J* 7.7 Hz), 10.53 (1H, s); ^{13}C NMR (75 MHz, $CDCl_3$) δ 14.0, 61.5, 65.6, 112.6, 121.8, 125.4, 128.5, 135.7, 160.1, 168.1, 189.5.

4.6.7. Synthesis of ethyl 2-(1-formylnaphth-2-yloxy)acetate (15)

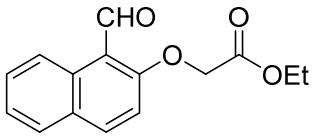

15

2-Hydroxynaphthaldehyde (**14**) (5.17 g, 30 mmol) was added to a suspension of potassium carbonate (4.56 g, 33 mmol) in acetone (115 mL). The mixture was stirred for 5 min at room temperature under an argon atmosphere. Ethyl 2-bromoacetate (5.51 g, 3.66 mL, 33 mmol) was added to the reaction mixture and the mixture was refluxed for 4 h. After cooling, the reaction mixture was filtered and the residue was washed with acetone. The filtrate was evaporated in vacuo to give the crude product as a light brown solid. The crude product was recrystallised from ethanol to give compound **15** as beige solid (3.72 g, 48%) R_f*:* 0.19 (10% EtOAc in LP, UV and $KMnO_4$ dip). ESI – MS, m/z: 281 $[M + Na]^+$. HRMS calculated for $C_{15}H_{14}NaO_4^+$ 281.0784, found 281.0789. ^{1}H NMR (300 MHz, $CDCl_3$) δ 1.27 (3H, t, *J* 7.1 Hz), 4.26 (2H, q, *J* 7.1 Hz), 4.85 (2H, s), 7.10 (1H, d, *J* 9.1 Hz), 7.39 – 7.45 (1H, m), 7.58 – 7.64 (1H, m), 7.75 (1H, dt, *J* 0.7 Hz, *J* 1.3 Hz, *J* 8.1 Hz), 8.01 (1H, d, *J* 9.1 Hz), 9.24 – 9.28 (1H, m) in agreement with that described by Yeap *et al.* [72]; ^{13}C NMR (75 MHz, $CDCl_3$) δ 14.1, 61.7, 66.4, 113.2, 117.7, 125.14, 125.19, 128.2, 129.1, 129.9, 131.4, 137.3, 162.0, 168.2, 192.1.

4.6.8. Synthesis of (2*R*/2*S*, 4*R*)-methyl 2-(2-(2-ethoxy-2-oxoethoxy)phenyl)thiazolidine-4-carboxylate (11g)

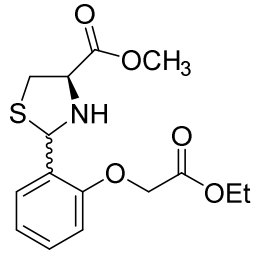

11g

L-Cysteine (**9**) was dissolved in ethanol:water (1:1) (15 mL). Sodium bicarbonate (1.14 g, 13.61 mmol) was added, and after 10 min, the aromatic aldehyde **13** (2.58 g, 12.38 mmol) was added and stirred for 14 h. Ethanol was evaporated in vacuo and DCM (50 mL) was added and washed with water (25 mL), dried over Na_2SO_4, filtered and evaporated in vacuo to afford the crude product of **11g**. The crude product was purified by silica flash column chromatography (10-60% EtOAc in LP) to afford *cis* and *trans* mixture of **11g** as a brown solid (484 mg, 12%) R_f*:* 0.28 (30% EtOAc in LP, UV and $KMnO_4$ dip). ESI – MS, m/z: 348 $[M + Na]^+$. HRMS calculated for $C_{15}H_{19}NNaO_5S^+$ 348.0876, found 348.0881. ^{1}H NMR (400 MHz, $CDCl_3$) δ 1.12 – 1.20 (3H, m), 2.99 – 3.07 (1H, m), 3.21 – 3.34 (1H, m), 3.67 – 3.68 (3H, m), 3.85 (0.5H, t, *J* 15.6 Hz), 4.10 – 4.17 (2H, m), 4.23 – 4.26 (0.5H, m), 4.55 – 4.57 (2H, m), 5.78 (0.5H, s), 5.94 (0.5H, s), 6.68 (1H, dd, *J* 8.3 Hz, *J* 18.2 Hz), 6.83 – 6.92 (1H, m), 7.08 – 7.18 (1H, m), 7.33 (0.5H, d, *J* 7.6 Hz), 7.39 (0.5H, d, *J* 7.6 Hz); ^{13}C NMR (100 MHz, $CDCl_3$) δ 13.76, 13.78, 37.3, 38.4, 52.01, 52.04, 60.9, 64.8, 65.3, 65.4, 65.6, 66.5, 67.4, 111.7, 112.0, 121.2, 121.5, 126.6, 126.7, 128.1, 128.4, 129.3, 129.8, 154.9, 155.3, 168.0, 168.2, 171.1, 171.8.

4.6.9. Synthesis of (2*R*/2*S*, 4*R*)-methyl 2-(2-(2-ethoxy-2-oxoethoxy)naphth-1-yl)thiazolidine-4-carboxylate (11h)

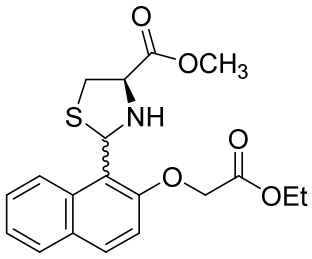

11h

L-Cysteine (**9**) was dissolved in ethanol : water (1:1) (15 mL). Sodium bicarbonate (1.32 g, 15.69 mmol) was added, and after 10 min, the aromatic aldehyde **15** (3.68 g, 14.26 mmol) was added to form a white precipitate immediately. The reaction mixture was filtered using ethanol : water (1:1). The residue was taken up with DCM (100 mL) and washed with water (25 mL), dried over Na_2SO_4, filtered and evaporated in vacuo to afford the crude product of **11h**. The crude product was purified by suspending it in ether (100 mL), filter and the residue was washed thoroughly with ether to afford a mixture of *cis* and *trans* **11h** as a white solid (4.12 g, 77%) R_f*:* 0.29 (30% EtOAc in LP, UV and $KMnO_4$ dip). ESI – MS, m/z: 398 $[M + Na]^+$. HRMS calculated for $C_{19}H_{21}NNaO_5S^+$ 398.1033, found 398.1043. ^{1}H NMR (500 MHz, $CDCl_3$) δ 1.26 – 1.32 (3H, m), 3.27 (1H, t, *J* 10.0 Hz), 3.51 – 3.55 (1H, m), 3.59 (0.4H, dd, *J* 2.0 Hz, *J* 10.5 Hz), 3.81 (s) and 3.82 (s) integrate for (3H), 4.01 – 4.04 (0.6H, m), 4.25 – 4.29 (2H, m), 4.72 – 4.85 (2H, m), 6.53 (s) and 6.59 (s) integrate for (1H), 7.13 (1H, dd, *J* 9.0 Hz, *J* 16.5 Hz), 7.37 – 7.39 (1H, m), 7.49 – 7.53 (1H, m), 7.75 – 7.81 (2H, m), 8.10 (1H, dd, *J* 3.0 Hz, *J* 8.5 Hz); ^{13}C NMR (125 MHz, $CDCl_3$) δ 14.15, 14.18, 38.5, 39.2, 52.41, 52.43, 61.5, 61.6, 65.6, 66.0, 66.2, 66.6, 66.8, 66.9, 114.7, 114.9, 118.7, 119.1, 122.6, 122.9, 124.3, 124.4, 127.3, 127.4, 128.5, 128.8, 129.8, 130.5, 130.7, 132.3, 132.5, 154.1, 154.3, 168.3, 168.6, 171.3, 172.7.

4.6.10. Synthesis of methyl 2-(2-(2-ethoxy-2-oxoethoxy)phenyl)thiazole-4-carboxylate (12g)

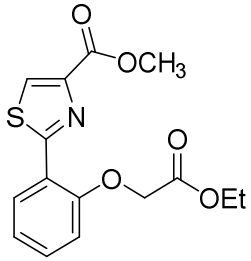

12g

This compound **12g** was prepared using the general method described by Gududuru *et al.* [35]. NBS (2.1 eq, 556 mg, 3.12 mmol) and benzoyl peroxide (0.03 eq, 11 mg, 0.045 mmol) were added to a solution of **11g** (483 mg, 1.49 mmol) in CCl_4 (15 mL). The reaction mixture was refluxed for 14 h. The hot mixture was filtered and evaporated in vacuo. The crude product was purified by silica flash column chromatography (10-60% EtOAc in LP) to afford the corresponding thiazole derivative **12g** as a brown solid (80 mg, 17%) R_f *:* 0.37 (30% EtOAc in LP, UV and $KMnO_4$ dip). ESI – MS, m/z: 344 $[M + Na]^+$. HRMS calculated for $C_{15}H_{15}NNaO_5S^+$ 344.0563, found 344.0565. ^{1}H NMR (400 MHz, $CDCl_3$) δ 1.24 (3H, t, *J* 7.1 Hz), 3.92 (3H, s), 4.24 (2H, q, *J* 7.1 Hz), 4.78 (2H, s), 6.86 (1H, dd, *J* 0.9 Hz, *J* 8.5 Hz), 7.06 – 7.10 (1H, m), 7.31 – 7.35 (1H, m), 8.20 (1H, s), 8.47 (1H, dd, *J* 1.7 Hz, *J* 7.9 Hz); ^{13}C NMR (100 MHz, $CDCl_3$) δ 14.0, 52.2, 61.5, 65.6, 111.8, 121.9, 122.0, 128.5, 129.4, 131.2, 145.6, 154.6, 162.2, 162.8, 167.8.

4.6.11. Synthesis of methyl 2-(2-(2-ethoxy-2-oxoethoxy)naphth-1-yl)thiazole-4-carboxylate (12h)

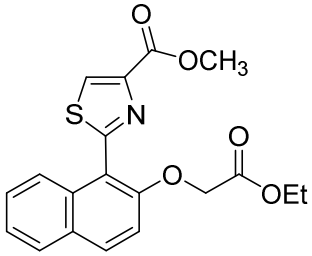

12h

This compound **12h** was prepared using the general method described by Gududuru *et al.* [35]. NBS (2.1 eq, 2.78 g, 15.60 mmol) and benzoyl peroxide (0.03 eq, 55 mg, 0.23 mmol) were added to a solution of **11h** (2.81 g, 7.50 mmol) in CCl_4 (75 mL) and the reaction mixture was refluxed for 14 h. The hot mixture was filtered and evaporated in vacuo. The crude product was purified by silica flash column chromatography (10-60% EtOAc in LP) to afford the corresponding thiazole derivative **12h** as a brown solid (211 mg, 8%) R_f *:* 0.34 (30% EtOAc in LP, UV and $KMnO_4$ dip). ESI – MS, m/z: 394 $[M + Na]^+$. HRMS calculated for $C_{19}H_{17}NNaO_5S^+$ 394.0720, found 394.0727.^{1}H NMR (300 MHz, $CDCl_3$) δ 1.19 (3H, t, *J* 7.1 Hz), 3.92 (3H, s), 4.16 (2H, q, *J* 7.1 Hz), 4.68 (2H, s), 7.14 (1H, d, *J* 9.1 Hz), 7.31 – 7.37 (1H, m), 7.40 – 7.47 (1H, m), 7.74 (1H, d, *J* 8.7 Hz), 7.86 (1H, d, *J* 9.0 Hz), 7.96 (1H, d, *J* 8.6 Hz), 8.40 (1H, s); ^{13}C NMR (75 MHz, $CDCl_3$) δ 13.9, 52.2, 61.2, 66.3, 113.2, 116.5, 124.5, 124.7, 127.8, 129.2, 129.4, 132.1, 132.9, 146.3, 153.7, 162.0, 162.9, 168.3.

4.6.12. Synthesis of 2-(2-(carboxymethoxy)phenyl)thiazole-4-carboxylic acid (4g)

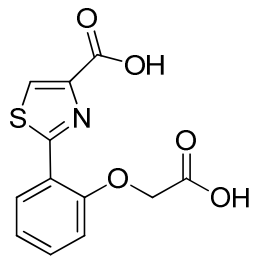

4g

This compound **4g** was prepared using the general method described by Gududuru *et al.* [35]. Sodium hydroxide solution (1 M, 3 mL) was added to a solution of the thiazole methyl ester

derivative **12g** (80 mg, 0.25 mmol) in methanol (6 mL). The solution was stirred for 4 h, and then methanol was evaporated in vacuo. The solution was acidified with conc HCl and extracted with EtOAc (3 x 50 mL). The combined organic layer was washed with brine (50 mL), water (50 mL), dried over Na_2SO_4, and evaporated in vacuo to afford the corresponding carboxylic acid derivative **4g** as a brown solid (51 mg, 73%). ESI – MS, m/z: 300 [M + Na - 2H]$^-$. HRMS calculated for $C_{12}H_7NNaO_5S^-$ 299.9948, found 299.9956. ^{1}H NMR (500 MHz, DMSO) δ 4.99 (2H, s), 7.15 (2H, dd, *J* 8.9 Hz, *J* 17.6Hz), 7.45 (1H, dt, *J* 1.7 Hz, *J* 8.7 Hz, *J* 9.7 Hz), 8.29 (1H, dd, *J* 1.7 Hz, *J* 7.9 Hz), 8.51 (1H, s); ^{13}C NMR (125 MHz, DMSO) δ 65.1, 113.0, 121.2, 121.5, 128.0, 129.5, 131.5, 146.2, 154.8, 161.7, 162.4, 169.6.

4.6.13. Synthesis of 2-(2-(carboxymethoxy)naphth-1-yl)thiazole-4-carboxylic acid (4h)

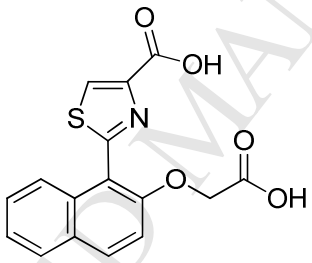

4h

4h was prepared using the general method described by Gududuru *et al.* [35]. Sodium hydroxide solution (1 M, 6 mL) was added to a solution of the thiazole methyl ester derivative **12h** (143 mg, 0.39 mmol) in methanol (6 mL). The solution was stirred for 4 h, and then methanol evaporated in vacuo. The solution was acidified with conc HCl and extracted with EtOAc (3 x 50 mL). The combined organic layers were washed with brine (50 mL) and water (50 mL), the dried over Na_2SO_4, filtered and evaporated in vacuo to afford the corresponding carboxylic acid derivative **4h** as a yellow solid (101 mg, 80%). ESI – MS, m/z: 350 [M + Na - 2H]$^-$. HRMS calculated for $C_{16}H_9NNaO_5S^-$ 350.0105, found 350.0102. ^{1}H NMR (500 MHz, DMSO) δ 4.97 (2H, s), 7.42 – 7.45 (1H, m), 7.48 – 7.53 (2H, m), 7.94 (1H, d, *J* 7.6 Hz), 8.07

– 8.10 (2H, m), 8.68 (1H, s); ^{13}C NMR (125 MHz, DMSO) δ 65.2, 113.9, 115.0, 124.3, 124.4, 127.9, 128.2, 128.7, 130.4, 132.1, 146.8, 154.0, 162.0, 162.4, 170.0.

4.6.14. General method for preparation of 2-aryl-1,3-thiazolidine-4-carboxylic acids (16a-c and 16f-j)

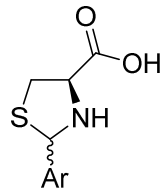

16a-c and **16f-j**

16a-c and **16f-j** were prepared using the general method described by Gududuru *et al.* [35]. A mixture of L-cysteine (**8**) (0.5 g, 4.12 mmol) and appropriate aryl aldehyde **(10a-c and 10f-j)** (4.12 mmol) in ethanol (15 mL) was stirred at room temperature for 5 h, and the solid separated was collected by filtration, washed with diethyl ether and dried to afford **16a-c** and **16f-j**.

4.6.14.1. (2*R*/2*S*, 4*R*)-2-(*p*-tolyl)thiazolidine-4-carboxylic acid (16a) [35]

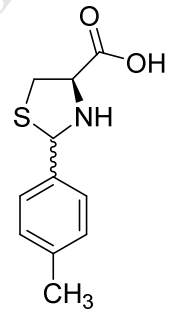

16a

16a was obtained as a white solid (582 mg, 63%). ^{1}H NMR (400 MHz, DMSO-d6) δ 2.27 (s) and 2.29 (s) integrate for 3H, 2.79 (0.3H, dd, *J* 6.5 Hz, *J* 14.0 Hz), 2.89 (0.4H, dd, *J* 4.2 Hz, *J* 14.0 Hz), 3.05 (0.6H, dd, *J* 8.7 Hz, *J* 10.0 Hz), 3.12 (0.7H, dd, *J* 4.5 Hz, *J* 10.3 Hz), 3.27 (0.7H, dd, *J* 7.2 Hz, *J* 10.2 Hz), 3.35 (0.7H, dd, *J* 7.2 Hz, *J* 10.1 Hz), 3.44 (0.4H, dd, *J* 4.2 Hz,

J 6.4 Hz), 3.85 (0.6H, dd, *J* 7.1 Hz, *J* 8.6 Hz), 4.21 (0.6H, dd, *J* 4.5 Hz, *J* 7.1 Hz), 5.45 (0.5H, s), 5.62 (0.6H, s), 7.12 (1H, d, *J* 7.8 Hz), 7.16 (1H, d, *J* 7.8 Hz), 7.30 (1H, d, *J* 8.1 Hz), 7.37 (1H, d, *J* 8.1 Hz) in agreement with that described by [35]; ^{13}C NMR (100 MHz, DMSO-d6) δ 20.6, 20.7, 37.9, 38.5, 64.9, 65.5, 71.0, 71.7, 126.8, 127.1, 128.7, 129.0, 135.9, 136.7, 137.6, 138.1, 172.3, 173.0.

4.6.14.2. (2*R*/2*S*, 4*R*)-2-phenylthiazolidine-4-carboxylic acid (16b) [35]

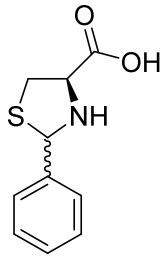

16b

16b was obtained as a white solid (570 mg, 66%). ^{1}H NMR (400 MHz, DMSO-d6) δ 3.05 – 3.14 (1H, m), 3.27 – 3.39 (1H, m), 3.87 – 3.91 (0.4H, m), 4.21 (0.5H, m), 5.49 (0.4H, s), 5.67 (0.5H, s), 7.26 – 7.51 (5H, m) in agreement with that described in the literature [35]; ^{13}C NMR (100 MHz, DMSO-d6) δ 38.0, 38.5, 64.9, 65.5, 71.0, 71.8, 126.9, 127.2, 127.5, 128.18, 128.24, 128.4, 138.9, 141.3, 172.3, 172.9.

4.6.14.3. (2*R*/2*S*, 4*R*)-2-(4-methoxyphenyl)thiazolidine-4-carboxylic acid (16c) [35]

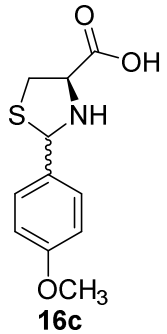

16c

16c was obtained as a white solid (516 mg, 52%). ^{1}H NMR (400 MHz, DMSO-d6) δ 2.79 (0.6H, dd, *J* 6.5 Hz, *J* 14.0 Hz), 2.89 (0.6H, dd, *J* 4.2 Hz, *J* 14.0 Hz), 3.04 (0.8H, dd, *J* 8.7 Hz,

J 10.0 Hz), 3.13 (0.8H, dd, *J* 4.2 Hz, *J* 10.3 Hz), 3.27 (1H, dd, *J* 7.2 Hz, *J* 10.2 Hz), 3.35 (1H, dd, *J* 7.2 Hz, *J* 10.1 Hz), 3.43 (1H, dd, *J* 4.1 Hz, *J* 6.4 Hz), 3.73 (s) and 3.74 (s) integrate for 3H, 3.84 (0.8H, dd, *J* 7.2 Hz, *J* 8.7 Hz), 4.22 (0.7H, dd, *J* 4.2 Hz, *J* 7.1 Hz), 5.44 (0.5H, s), 5.59 (0.5H, s), 6.87 (1H, d, *J* 8.7 Hz), 6.91 (1H, d, *J* 8.7 Hz), 7.35 (1H, d, *J* 8.7 Hz), 7.42 (1H, d, *J* 8.7 Hz) in agreement with that described in the literature [35]; ^{13}C NMR (100 MHz, DMSO-d6) δ 37.9, 38.6, 55.09, 55.14, 64.8, 65.5, 71.0, 71.6, 113.6, 113.8, 128.3, 128.6, 130.7, 132.8, 158.7, 159.2, 172.3, 173.1.

4.6.14.4. (2*R*/2*S*, 4*R*)-2-(naphth-1-yl)thiazolidine-4-carboxylic acid (16f)

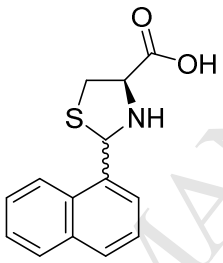

16f

16f was obtained as a white solid (728 mg, 68%). ^{1}H NMR (400 MHz, DMSO-d6) δ 2.82 (0.7H, dd, *J* 6.4 Hz, *J* 14.0 Hz), 2.91 (0.8H, dd, *J* 4.0 Hz, *J* 14.0 Hz), 3.06 – 3.12 (2H, m), 3.32 (2H, dd, *J* 6.8 Hz, *J* 10.0 Hz), 3.44 - 3.48 (2H, m), 4.07 (1H, dd, *J* 7.2 Hz, *J* 8.8 Hz), 4.26 (1H, t, *J* 6.4 Hz), 6.27 (0.5H, s), 6.44 (1H, s), 7.47 – 7.61 (5H, m), 7.74 (1H, d, *J* 7.2 Hz), 7.84 – 7.98 (4H, m), 8.08 (1H, d, *J* 8.4 Hz), 8.19 (0.5H, d, *J* 8.3 Hz); ^{13}C NMR (100 MHz, DMSO-d6) δ 37.8, 38.1, 55.8, 65.1, 65.4, 68.0, 68.3, 122.3, 123.3, 123.5, 123.6, 125.3, 125.5, 125.7, 125.9, 126.1, 126.3, 127.7, 128.4, 128.6, 130.4, 130.7, 133.2, 133.3, 134.6, 137.2, 172.4, 173.0. NMR spectra are in agreement with those reported by Schneider *et al.* [73].

4.6.14.5. (2*R*/2*S*, 4*R*)-2-(2-hydroxynaphth-1-yl)thiazolidine-4-carboxylic acid (16g)

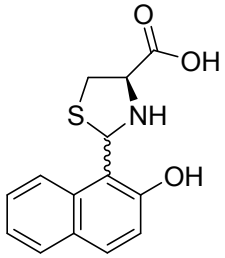

16g

16g was obtained as a yellow solid (793 mg, 70%). ^{1}H NMR (500 MHz, DMSO-d6) δ 2.76 (1H, dd, *J* 6.6 Hz, *J* 13.9 Hz), 2.87 (1H, dd, *J* 4.2 Hz, *J* 14.1 Hz), 3.11 (1H, t, *J* 9.2 Hz), 3.22 (1H, dd, *J* 4.3 Hz, *J* 10.7 Hz), 3.36 (2H, dd, *J* 4.2 Hz, *J* 6.7 Hz), 3.40 - 3.44 (2H, m), 3.98 (0.5H, t, *J* 7.6 Hz), 4.43 (0.3H, t, *J* 5.3 Hz), 6.34 (0.5H, s), 6.47 (0.3H, s), 7.03 (1H, dd, *J* 8.8 Hz, *J* 39.2 Hz), 7.28 (1H, t, *J* 7.3 Hz), 7.45 (1H, t, *J* 7.6 Hz), 7.69 – 7.79 (2H, m), 7.91 (0.5H, d, *J* 8.6 Hz); ^{13}C NMR (125 MHz, DMSO-d6) δ 26.3, 40.7, 56.4, 74.3, 120.1, 122.1, 127.2, 168.4.

4.6.14.6. (2*R*/2*S*, 4*R*)-2-(4-hydroxyphenyl)thiazolidine-4-carboxylic acid (16h)

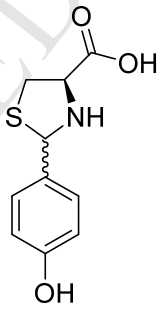

16h

16h was obtained as a white solid (592 mg, 64%). ^{1}H NMR (400 MHz, DMSO-d6) δ 2.82 (0.3H, dd, *J* 6.4 Hz, *J* 14.1 Hz), 2.90 (0.3H, dd, *J* 4.2 Hz, *J* 14.1 Hz), 3.03 (0.6H, dd, *J* 8.7 Hz, *J* 10.0 Hz), 3.13 (0.6H, dd, *J* 4.0 Hz, *J* 10.2 Hz), 3.26 (0.6H, dd, *J* 7.3 Hz, *J* 10.3 Hz), 3.34 (0.6H, dd, *J* 7.2 Hz, *J* 10.1 Hz), 3.50 (0.3H, dd, *J* 4.2 Hz, *J* 6.3 Hz), 3.81 (0.8H, dd, *J* 7.3 Hz, *J* 8.6 Hz), 4.23 (0.5H, dd, *J* 4.0 Hz, *J* 7.2 Hz), 5.39 (0.5H, s), 5.53 (0.5H, s), 6.69 (1H, d, *J* 8.6 Hz), 6.73 (1H, d, *J* 8.5 Hz), 7.23 (1H, d, *J* 8.6 Hz), 7.29 (1H, d, *J* 8.5 Hz) in agreement with

that described by Song *et al.* [74]; ^{13}C NMR (100 MHz, DMSO-d6) δ 37.8, 38.6, 64.8, 65.4, 71.3, 71.9, 114.9, 115.2, 128.3, 128.5, 128.8, 130.8, 156.9, 157.4, 172.4, 173.2.

4.6.14.7. (2*R*/2*S*, 4*R*)-2-(2-hydroxyphenyl)thiazolidine-4-carboxylic acid (16i)

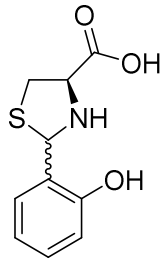

16i

16i was obtained as a white solid (865 mg, 93%). ^{1}H NMR (400 MHz, DMSO-d6) δ 2.96 (1H, dd, *J* 9.1 Hz, *J* 9.9 Hz), 3.01 (1H, dd, *J* 5.3 Hz, *J* 10.2 Hz), 3.19 (1H, dd, *J* 6.8 Hz, *J* 10.1 Hz), 3.33 (1H, dd, *J* 6.9 Hz, *J* 10.0 Hz), 3.82 (1H, dd, *J* 7.0 Hz, *J* 9.0 Hz), 4.20 (1H, dd, *J* 5.4 Hz, *J* 6.6 Hz), 5.64 (1H, s), 5.83 (1H, s), 6.73 – 6.82 (4H, m), 7.03 – 7.07 (1H, m), 7.10 – 7.14 (1H, m), 7.28 (1H, dd, *J* 1.6 Hz, *J* 7.5 Hz), 7.33 (1H, dd, *J* 1.6 Hz, *J* 7.6 Hz); ^{13}C NMR (100 MHz, DMSO-d6) δ 37.1, 38.2, 64.8, 65.2, 65.6, 67.7, 115.1, 115.7, 118.7, 119.0, 124.2, 126.1, 127.6, 127.9, 128.1, 129.0, 154.6, 155.2, 172.5, 172.9. NMR spectra are in agreement with those reported by Jagtap *et al.* [75].

4.6.14.8. (2*R*/2*S*, 4*R*)-2-(furan-2-yl)thiazolidine-4-carboxylic acid (16j)

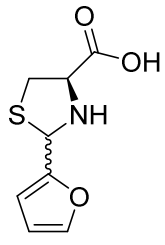

16j

16j was obtained as a very light brown solid (541 mg, 66%). ^{1}H NMR (400 MHz, DMSO-d6) δ 2.96 – 3.00 (1.6H, m), 3.28 (1H, dd, *J* 6.8 Hz, *J* 10.1 Hz), 3.34 (0.6H, dd, *J* 7.0 Hz, *J* 10.0

Hz), 3.85 (0.7H, dd, *J* 7.0 Hz, *J* 8.9 Hz), 4.10 (1H, t, *J* 6.4 Hz), 5.59 (0.6H, s), 5.74 (1H, s), 6.33 – 6.34 (1H, m), 6.37 (1H, dd, *J* 1.9 Hz, *J* 3.2 Hz), 6.43 (0.5H, dd, *J* 1.8 Hz, *J* 3.3 Hz), 6.49 (0.5H, d, *J* 3.4 Hz), 7.57 (1H, dd, *J* 0.9 Hz, *J* 1.9 Hz), 7.64 (0.5H, dd, *J* 0.8 Hz, *J* 1.9 Hz); ^{13}C NMR (100 MHz, DMSO-d6) δ 37.8, 38.0, 63.9, 64.2, 64.7, 65.2, 106.3, 107.5, 110.3, 110.6, 142.5, 142.9, 151.3, 154.4, 172.1, 172.5. NMR spectra are in agreement with those described by Braga *et al.* [76].

Acknowledgments

We thank Dr. Tri Le for assistance with NMR studies and Mr. Graham MacFarlane for MS measurements. This work was funded by Australian Research Council (DP0986292) and (DP150104358).

Supplementary data

Kinetic assays for compounds **4a-f**; ^{1}H and ^{13}C NMR spectra for all compounds.

References

1. N. Mitic, S.J. Smith, A. Neves, L.W. Guddat, L.R. Gahan, G. Schenk, *The catalytic mechanisms of binuclear metallohydrolases*, Chem. Rev. 106 (**2006**) 3338-3363.
2. G. Schenk, N. Mitic, L.R. Gahan, D.L. Ollis, R.P. McGeary, L.W. Guddat, *Binuclear metallohydrolases: complex mechanistic strategies for a simple chemical reaction*, Acc. Chem. Res. 45 (**2012**) 1593-1603.
3. G. Schenk, N. Mitic, G.R. Hanson, P. Comba, *Purple acid phosphatase: A journey into the function and mechanism of a colorful enzyme*, Coordin. Chem. Rev. 257 (**2013**) 473-482.
4. N. Mitic, M. Miraula, C. Selleck, K.S. Hadler, E. Uribe, M.M. Pedroso, G. Schenk, *Catalytic mechanisms of metallohydrolases montaining two metal ions*, In *Advances in Protein Chemistry and Structural Biology: Metal-containing Enzymes (Christov C.Z., Ed.)* ed., Vol. 97; Elsevier: Oxford, **2014**, pp 49-81.
5. A. Reithmeier, T. Lundbaeck, M. Haraldsson, M. Frank, B. Ek-Rylander, P.-G. Nyholm, A.-L. Gustavsson, G. Andersson, *Identification of inhibitors of Tartrate-resistant acid phosphatase (TRAP/ACP5) activity by small-molecule screening*, Chem. Biol. Drug Des. (**2018**) Ahead of Print.
6. B.C. Antanaitis, P. Aisen, *Uteroferrin and the purple acid-phosphatases*, Adv. Inorg. Biochem. 5 (**1983**) 111-136.
7. A.R. Hayman, T.M. Cox, *Purple acid-phosphatase of the human macrophage and osteoclast - characterization, molecular-properties, and crystallization of the recombinant di-iron-oxo protein secreted by baculovirus-infected insect cells*, J. Biol. Chem. 269 (**1994**) 1294-1300.
8. S.J. Smith, A. Casellato, K.S. Hadler, N. Mitic, M.J. Riley, A.J. Bortoluzzi, B. Szpoganicz, G. Schenk, A. Neves, L.R. Gahan, *The reaction mechanism of the Ga(III)Zn(II) derivative of uteroferrin and corresponding biomimetics*, J. Biol. Inorg. Chem. 12 (**2007**) 1207-1220.
9. G. Schenk, R.A. Peralta, S.C. Batista, A.J. Bortoluzzi, B. Szpoganicz, A.K. Dick, P. Herrald, G.R. Hanson, R.K. Szilagyi, M.J. Riley, L.R. Gahan, A. Neves, *Probing the role of the divalent metal ion in uteroferrin using metal ion replacement and a comparison to isostructural biomimetics*, J. Biol. Inorg. Chem. 13 (**2008**) 139-155.
10. N. Mitic, C.J. Noble, L.R. Gahan, G.R. Hanson, G. Schenk, *Metal-ion mutagenesis: conversion of a purple acid phosphatase from sweet potato to a neutral phosphatase with the formation of an unprecedented catalytically competent (MnMnII)-Mn-II active site*, J. Am. Chem. Soc. 131 (**2009**) 8173-8179.
11. N. Mitic, K.S. Hadler, L.R. Gahan, A.C. Hengge, G. Schenk, *The divalent metal Ion in the active site of uteroferrin modulates substrate binding and catalysis*, J. Am. Chem. Soc. 132 (**2010**) 7049-7054.
12. G. Schenk, C.L. Boutchard, L.E. Carrington, C.J. Noble, B. Moubaraki, K.S. Murray, J. de Jersey, G.R. Hanson, S. Hamilton, *A purple acid phosphatase from sweet potato contains an antiferromagnetically coupled binuclear Fe-Mn center*, J. Biol. Chem. 276 (**2001**) 19084-19088.
13. N. Mitic, M. Valizadeh, E.W.W. Leung, J. de Jersey, S. Hamilton, D.A. Hume, A.I. Cassady, G. Schenk, *Human tartrate-resistant acid phosphatase becomes an effective ATPase upon proteolytic activation*, Arch. Biochem. Biophys. 439 (**2005**) 154-164.
14. K. Hollberg, K. Hultenby, A.R. Hayman, T.M. Cox, G. Andersson, *Osteoclasts from mice deficient in tartrate-resistant acid phosphatase have altered ruffled borders and disturbed intracellular vesicular transport*, Exp. Cell Res. 279 (**2002**) 227-238.
15. G.W. Oddie, G. Schenk, N.Z. Angel, N. Walsh, L.W. Guddat, J. De Jersey, A.I. Cassady, S.E. Hamilton, D.A. Hume, *Structure, function, and regulation of tartrate-resistant acid phosphatase*, Bone 27 (**2000**) 575-584.

16. P.R. Nuttleman, R.M. Roberts, *Transfer of iron from uteroferrin (purple acid-phosphatase) to transferrin related to acid-phosphatase-activity*, J. Biol. Chem. 265 (**1990**) 12192-12199.
17. B.P. Gaber, J.P. Sheridan, F.W. Bazer, R.M. Roberts, *Resonance Raman-scattering from uteroferrin, the purple glycoprotein of the porcine uterus*, J. Biol. Chem. 254 (**1979**) 8340-8342.
18. P. Ling, R.M. Roberts, *Uteroferrin and Intracellular Tartrate-Resistant Acid-Phosphatases Are the Products of the Same Gene*, J. Biol. Chem. 268 (**1993**) 6896-6902.
19. M.B. Twitchett, G. Schenk, M.A.S. Aquino, D.T.Y. Yiu, T.C. Lau, A.G. Sykes, *Reactivity of M-II metal-substituted derivatives of pig purple acid phosphatase (Uteroferrin) with phosphate*, Inorg. Chem. 41 (**2002**) 5787-5794.
20. A.J. Janckila, D.H. Neustadt, Y.R. Nakasato, J.M. Halleen, T. Hentunen, L.T. Yam, *Serum tartrate-resistant acid phosphatase isoforms in rheumatoid arthritis*, Clin. Chim Acta 320 (**2002**) 49-58.
21. J.M. Halleen, S. Raisanen, J.J. Salo, S.V. Reddy, G.D. Roodman, T.A. Hentunen, P.P. Lehenkari, H. Kaija, P. Vihko, H.K. Vaananen, *Intracellular fragmentation of bone resorption products by reactive oxygen species generated by osteoclastic tartrate-resistant acid phosphatase*, J. Biol. Chem. 274 (**1999**) 22907-22910.
22. P.V. Bernhardt, G. Schenk, G.J. Wilson, *Direct electrochemistry of porcine purple acid phosphatase (uteroferrin)*, Biochemistry 43 (**2004**) 10387-10392.
23. H.C. Roberts, L. Knott, N.C. Avery, T.M. Cox, M.J. Evans, A.R. Hayman, *Altered collagen in tartrate-resistant acid phosphatase (TRAP)-deficient mice: A role for TRAP in bone collagen metabolism*, Calcified Tissue Int. 80 (**2007**) 400-410.
24. J.M. Halleen, H. Kaija, J.J. Stepan, P. Vihko, H.K. Vaananen, *Studies on the protein tyrosine phosphatase activity of tartrate-resistant acid phosphatase*, Arch. Biochem. Biophys. 352 (**1998**) 97-102.
25. A.R. Hayman, S.J. Jones, A. Boyde, D. Foster, W.H. Colledge, M.B. Carlton, M.J. Evans, T.M. Cox, *Mice lacking tartrate-resistant acid phosphatase (Acp 5) have disrupted endochondral ossification and mild osteopetrosis*, Development 122 (**1996**) 3151-3162.
26. J.U. Flanagan, A.I. Cassady, G. Schenk, L.W. Guddat, D.A. Hume, *Identification and molecular modeling of a novel, plant-like, human purple acid phosphatase*, Gene 377 (**2006**) 12-20.
27. D. Feder, W.M. Hussein, D.J. Clayton, M.W. Kan, G. Schenk, R.P. McGeary, L.W. Guddat, *Identification of purple acid phosphatase inhibitors by fragment-based screening: promising new leads for osteoporosis therapeutics*, Chem. Biol. Drug Des. 80 (**2012**) 665-674.
28. M. Valizadeh, G. Schenk, K. Nash, G.W. Oddie, L.W. Guddat, D.A. Hume, J. de Jersey, T.R. Burke, S. Hamilton, *Phosphotyrosyl peptides and analogues as substrates and inhibitors of purple acid phosphatases*, Arch. Biochem. Biophys. 424 (**2004**) 154-162.
29. T.W. Elliott, N. Mitic, L.R. Gahan, L.W. Guddat, G. Schenk, *Inhibition studies of purple acid phosphatases: Implications for the catalytic mechanism*, J. Braz. Chem. Soc. 17 (**2006**) 1558-1565.
30. J.K. Myers, S.M. Antonelli, T.S. Widlanski, *Motifs for metallophosphatase inhibition*, J. Am. Chem. Soc. 119 (**1997**) 3163-3164.
31. R.P. McGeary, P. Vella, J.Y.W. Mak, L.W. Guddat, G. Schenk, *Inhibition of purple acid phosphatase with alpha-alkoxynaphthylmethylphosphonic acids*, Bioorg. Med. Chem. Lett. 19 (**2009**) 163-166.
32. S.H. Mohd-Pahmi, W.M. Hussein, G. Schenk, R.P. McGeary, *Synthesis, modelling and kinetic assays of potent inhibitors of purple acid phosphatase*, Bioorg. Med. Chem. Lett. 21 (**2011**) 3092-3094.

33. Faridoon, W.M. Hussein, N.U. Islam, L.W. Guddat, G. Schenk, R.P. McGeary, *Penicillin inhibitors of purple acid phosphatase*, Bioorg. Med. Chem. Lett. 22 (**2012**) 2555-2559.
34. E.R. Zartler, M.J. Shapiro, *Fragonomics: fragment-based drug discovery*, Curr. Opin. Chem. Biol. 9 (**2005**) 366-370.
35. V. Gududuru, E. Hurh, J.T. Dalton, D.D. Miller, *Discovery of 2-arylthiazolidine-4-carboxylic acid amides as a new class of cytotoxic agents for prostate cancer*, J. Med. Chem. 48 (**2005**) 2584-2588.
36. M. Ashram, *Synthesis of calix 4 crowns containing soft donor atoms and a study of their metal-cation binding properties: highly selective receptors for Cu2+*, J. Chem. Soc., Perkin Trans. 2. (**2002**) 1662-1668.
37. D. Liebschner, P.V. Afonine, N.W. Moriarty, B.K. Poon, O.V. Sobolev, T.C. Terwilliger, P.D. Adams, *Polder maps: improving OMIT maps by excluding bulk solvent*, Acta Crystallogr. D-Str. Biol. 73 (**2017**) 148-157.
38. K.S. Hadler, N. Mitic, F. Ely, G.R. Hanson, L.R. Gahan, J.A. Larrabee, D.L. Ollis, G. Schenk, *Structural flexibility enhances the reactivity of the bioremediator glycerophosphodiesterase by fine-tuning its mechanism of hydrolysis*, J. Am. Chem. Soc. 131 (**2009**) 11900-11908.
39. M.M. Pedroso, J.A. Larrabee, F. Ely, S.E. Gwee, N. Mitic, D.L. Ollis, L.R. Gahan, G. Schenk, *Ca-II binding regulates and dominates the reactivity of a transition-metal-ion-dependent diesterase from mycobacterium tuberculosis*, Chem. Eur. J. 22 (**2016**) 999-1009.
40. N. Strater, B. Jasper, M. Scholte, B. Krebs, A.P. Duff, D.B. Langley, R.L. Han, B.A. Averill, H.C. Freeman, J.M. Guss, *Crystal structures of recombinant human purple acid phosphatase with and without an inhibitory conformation of the repression loop*, J. Mol. Biol. 351 (**2005**) 233-246.
41. C. Selleck, D. Clayton, L.R. Gahan, N. Mitic, R.P. McGeary, M.M. Pedroso, L.W. Guddat, G. Schenk, *Visualization of the reaction trajectory and transition state in a hydrolytic reaction catalyzed by a metalloenzyme*, Chem. Eur. J. 23 (**2017**) 4778-4781.
42. G. Schenk, T.W. Elliott, E. Leung, L.E. Carrington, N. Mitic, L.R. Gahan, L.W. Guddat, *Crystal structures of a purple acid phosphatase, representing different steps of this enzyme's catalytic cycle*, BMC Struct. Biol. 8 (**2008**).
43. G. Schenk, L.R. Gahan, L.E. Carrington, N. Mitic, M. Valizadeh, S.E. Hamilton, J. de Jersey, L.W. Guddat, *Phosphate forms an unusual tripodal complex with the Fe-Mn center of sweet potato purple acid phosphatase*, Proc. Natl. Acad. Sci. USA 102 (**2005**) 273-278.
44. J. Schindelmeiser, F. Gullotta, D. Munstermann, *Purple acid-phosphatase of human-brain macrophages in aids encephalopathy*, Pathol. Res. Pract. 185 (**1989**) 184-186.
45. J. Schindelmeiser, H.J. Radzun, D. Munstermann, *Tartrate-resistant, purple acid-phosphatase in gaucher cells of the spleen - immunochemical and cytochemical analysis*, Pathol. Res. Pract. 187 (**1991**) 209-213.
46. J.D. Hoyer, C.Y. Li, L.T. Yam, C.A. Hanson, P.J. Kurtin, *Immunohistochemical demonstration of acid phosphatase isoenzyme 5 (tartrate-resistant) in paraffin sections of hairy cell leukemia and other hematologic disorders*, Am. J. Clin. Pathol. 108 (**1997**) 308-315.
47. P. Lang, M. Schultzberg, G. Andersson, *Expression and distribution of tartrate-resistant purple acid phosphatase in the rat nervous system*, J. Histochem. Cytochem. 49 (**2001**) 379-396.
48. Y.C. Chung, C.H. Ku, T.Y. Chao, J.C. Yu, M.M. Chen, S.H. Lee, *Tartrate-resistant acid phosphatase 5b activity is a useful bone marker for monitoring bone metastases in breast cancer patients after treatment*, Cancer Epidem. Biomar. 15 (**2006**) 424-428.

49. L.B. Tanko, M.A. Karsdal, C. Christiansen, D.J. Leeming, *Biochemical approach to the detection and monitoring of metastatic bone disease: What do we know and what questions need answers?*, Cancer Metast. Rev. 25 (**2006**) 659-668.
50. J.L. Beck, L.A. Mcconachie, A.C. Summors, W.N. Arnold, J. Dejersey, B. Zerner, *Properties of a purple phosphatase from red kidney Bean - a zinc-iron metalloenzyme*, Biochim. Biophys. Acta 869 (**1986**) 61-68.
51. H.D. Campbell, D.A. Dionysius, D.T. Keough, B.E. Wilson, J.D. Jersey, B. Zerner, *Iron-containing acid-phosphatases - comparison of enzymes from beef spleen and pig allantoic fluid*, Biochem. Bioph. Res. Co. 82 (**1978**) 615-620.
52. CrystalClear (Rigaku, 2005) Rigaku Corporation, Tokyo, Japan.
53. S. Bailey, *The Ccp4 Suite - programs for protein crystallography*, Acta Crystallogr. D-Biol. Cryst. 50 (**1994**) 760-763.
54. P.D. Adams, P.V. Afonine, G. Bunkoczi, V.B. Chen, I.W. Davis, N. Echols, J.J. Headd, L.W. Hung, G.J. Kapral, R.W. Grosse-Kunstleve, A.J. McCoy, N.W. Moriarty, R. Oeffner, R.J. Read, D.C. Richardson, J.S. Richardson, T.C. Terwilliger, P.H. Zwart, *PHENIX: a comprehensive Python-based system for macromolecular structure solution*, Acta Crystallogr. D-Biol. Cryst. 66 (**2010**) 213-221.
55. P. Emsley, K. Cowtan, *Coot: model-building tools for molecular graphics*, Acta Crystallogr. D-Biol. Cryst. 60 (**2004**) 2126-2132.
56. S. McNicholas, E. Potterton, K.S. Wilson, M.E.M. Noble, *Presenting your structures: the CCP4mg molecular-graphics software*, Acta Crystallogr. D-Biol. Cryst. 67 (**2011**) 386-394.
57. R. Thomsen, M.H. Christensen, *MolDock: A new technique for high-accuracy molecular docking*, J. Med. Chem. 49 (**2006**) 3315-3321.
58. W.C. Still, M. Kahn, A. Mitra, *Rapid chromatographic technique for preparative separations with moderate resolution*, J. Org. Chem. 43 (**1978**) 2923-2925.
59. R. Leardini, H. McNab, M. Minozzi, D. Nanni, D. Reed, A.G. Wright, *Reactions of 1-(2-alkoxyphenyl)alkaniminyl radicals*, J. Chem. Soc., Perkin Trans. 1. (**2001**) 2704-2710.
60. A. Wang, Z. Yang, J. Liu, Q. Gui, X. Chen, Z. Tan, J.-C. Shi, *Pd-catalyzed reduction of aldehydes to alcohols using formic acid as the hydrogen donor*, Synth. Commun. 44 (**2014**) 280-288.
61. K. Fukatsu, R. Fujii, M. Kobayashi, J. Yonemori, T. Tanaka, T.P. TanakaTakeda Pharm Co Ltd (Take) WO2005051373-A1; EP1688138-A1; JP2005515854-X; US2008167378-A1
62. B. Paul, W. Korytnyk, *Cysteine derivatives with reactive groups as potential antitumor agents*, J. Med. Chem. 19 (**1976**) 1002-1007.
63. M. Anwar, M.G. Moloney, *Chiral bicyclic tetramates as non-planar templates for chemical library synthesis*, Chem. Biol. Drug Des. 81 (**2013**) 645-649.
64. M. Wang, D. Li, W. Zhou, L. Wang, *A highly efficient palladium-catalyzed desulfitative arylation of azoles with sodium arylsulfinates*, Tetrahedron 68 (**2012**) 1926-1930.
65. A.C. Dawsey, V. Li, K.C. Hamilton, J. Wang, T.J. Williams, *Copper-catalyzed oxidation of azolines to azoles*, Dalton Trans. 41 (**2012**) 7994-8002.
66. Y. Liu, Z. Li, Y.C. Xie, P. He, J.F. Qiao, X.Y. Fan, Y.G. Du, *Efficient one-pot synthesis of 2,4-disubstituted thiazoles and dimeric thiazoles directly from acyl chlorides and -azido disulfides*, Synthesis 49 (**2017**) 4876-4886.
67. A. Aliabadi, A. Foroumadi, M. Safavi, S.K. Ardestani, *Synthesis, cytotoxicity assessment, and molecular docking of 4-substituted-2-p-tolylthiazole derivatives as probable c-Src and erb tyrosine kinase inhibitors*, Croat. Chem. Acta 86 (**2013**) 245-251.
68. S.Z. Zhao, X.Q. Zhang, P. Wei, X. Su, L.Y. Zhao, M.Y. Wu, C.Z. Hao, C.C. Liu, D.M. Zhao, M.S. Cheng, *Design, synthesis and evaluation of aromatic heterocyclic derivatives as potent antifungal agents*, Eur. J. Med. Chem. 137 (**2017**) 96-107.

69. G.W. Shipps, C.C. Cheng, X. Huang, T.O. Fischmann, J.S. Duca, M. Richards, H. Zeng, B. Sun, P.A. Reddy, T.T. Wong, P.K. Tadikonda, M.A. Siddiqui, M.M. Labroli, C. Poker, T.J. Guzi, G.W.J. Shipps, C. Cheng, J. Duca, T. Fischmann, T. Guzi, M. Labroli, P. Reddy, G. Shipps, M. Siddiqui, P. Tadikonda, T. Wong, M.A. Labroli, C.S. PokerSchering Corp. WO2008054702-A1
70. L. Ma, T.J. Wang, M. Shi, P. Fu, H.Y. Pei, H.Y. Ye, *Synthesis, activity, and docking study of novel phenylthiazole-carboxamido acid derivatives as FFA2 agonists*, Chem. Biol. Drug Des. 88 (**2016**) 26-37.
71. J. Carpenter, Y. Wang, G. Wu, J.X. Feng, X.Y. Ye, C.L. Morales, M. Broekema, K.A. Rossi, K.J. Miller, B.J. Murphy, G.G. Wu, S.E. Malmstrom, A.V. Azzara, P.M. Sher, J.M. Fevig, A. Alt, R.L. Bertekap, M.J. Cullen, T.M. Harper, K. Foster, E. Luk, Q. Xiang, M.F. Grubb, J.A. Robl, D.A. Wacker, *Utilization of an active site mutant receptor for the identification of potent and selective atypical 5-HT2C receptor agonists*, J. Med. Chem. 60 (**2017**) 6166-6190.
72. G.Y. Yeap, Y.H. Chan, W.A.K. Mahmood, *Novel fluorometric turn on detection of aluminum by chalcone-based chemosensor in aqueous phase*, J. Fluoresc. 27 (**2017**) 2017-2022.
73. P.H. Schneider, H.S. Schrekker, C.C. Silveira, L.A. Wessjohann, A.L. Braga, *First generation cysteine- and methionine-derived oxazolidine and thiazolidine ligands for palladium-catalyzed asymmetric allylations*, Eur. J. Org. Chem. (**2004**) 2715-2722.
74. Z.C. Song, G.Y. Ma, P.C. Lv, H.Q. Li, Z.P. Xiao, H.L. Zhu, *Synthesis, structure and structure-activity relationship analysis of 3-tert-butoxycarbonyl-2-arylthiazolidine-4-carboxylic acid derivatives as potential antibacterial agents*, Eur. J. Med. Chem. 44 (**2009**) 3903-3908.
75. R.M. Jagtap, S.H. Thorat, R.G. Gonnade, A.A. Khan, S.K. Pardeshi, *X-ray crystal structures and anti-breast cancer property of 3-tert-butoxycarbonyl-2-arylthiazolidine-4-carboxylic acids*, New J. Chem. 42 (**2018**) 1078-1086.
76. A.L. Braga, H.R. Appelt, P.H. Schneider, O.E.D. Rodrigues, C.C. Silveira, L.A. Wessjohann, *New C-2-symmetric chiral disulfide ligands derived from (R)-cysteine*, Tetrahedron 57 (**2001**) 3291-3295.

Highlights **Revised Manuscript EJMECH-D-18-01046**

- A lead inhibitor against Purple acid phosphatase has been further developed.
- Compounds are active against both pig and red kidney bean Purple acid phosphatases.
- A crystal structure of an inhibitor in complex with the red kidney bean enzyme (2.40 Å) is reported.